Selective autophagy in host defense against mycobacterial infection

Zhang, R.

Chapter 2

Dram1 deficiency leads to increased susceptibility of zebrafish to mycobacterial infection due to activation of pyroptotic cell death in infected macrophages

Rui Zhang, Monica Varela, Vincenzo Torraca, Michiel van der Vaart and Annemarie H. Meijer

(Manuscript in preparation)

Abstract

Mycobacterium tuberculosis (Mtb) and *Mycobacterium marinum* (Mm) are infectious bacterial pathogens and the causative agents of tuberculosis (TB) in humans and fish, respectively. These mycobacteria can survive and proliferate inside host macrophages. In response, infected macrophages elicit diverse mechanisms in an attempt to eliminate the intracellular pathogens and prevent further dissemination. There are many factors – both host and bacteria derived – that together determine the fate of a mycobacterium-infected macrophage: will it kill the pathogen, or succumb to the infection? The autophagy and cell death mediator DRAM1 was previously linked to autophagic host defense against mycobacterial infection. In this study, we found that CRISPR/Cas9-mediated mutation of zebrafish Dram1 does not reduce basal levels of autophagy under non-infected conditions. However, in the zebrafish larval model of TB, Dram1 deficiency reduces autophagic targeting of Mm and results in increased susceptibility to infection. Moreover, we demonstrate that Dram1, which is predominantly localized to lysosomal membranes, is required for acidification of Mm-containing vesicles. By *in vivo* imaging of the infection process, we observed that Dram1-deficient macrophages fail to restrict Mm during early stages of the infection. Knockdown of the zebrafish functional homolog of Caspase 1 could rescue the increased infection levels of Dram1 mutants. Therefore, extending the previously described function of Dram1 in maturation of mycobacteria-containing vesicles, we now propose that the presence of functional Dram1 limits pyroptotic cell death of mycobacteria-infected macrophages and thereby contributes to host resistance to mycobacterial infection.

Introduction

Tuberculosis (TB), caused by *Mycobacterium tuberculosis* (Mtb), remains a severe infectious disease and global health threat. The increase in drug-resistant Mtb strains and the occurrence of comorbidities, like co-infection with HIV, lower the effectiveness of current TB treatments [1, 2]. Thus, it is essential to fully understand the mechanisms of Mtb pathogenesis and develop novel approaches to improve the outcome of TB treatment. Autophagy is a conserved process that maintains cellular homeostasis by degrading unwanted cytoplasmic contents [3]. Various studies have demonstrated that autophagy also acts as an innate immune defense mechanism to

control mycobacterial infection [4-8]. Therefore, enhancing autophagic defenses forms a promising target for host-directed TB treatment [9, 10].

Many autophagy factors involved in defense against mycobacterial infection have been identified. DNA Damage Regulated Autophagy Modulator 1 (DRAM1) is a more recently discovered regulator of autophagy and cell death [11, 12]. Besides being involved in cancer and HIV infection [11, 13], a role for DRAM1 has been identified in defense against mycobacterial infections [7]. Transient knockdown of zebrafish *dram1* leads to decreased autophagic targeting of mycobacteria and increased susceptibility to mycobacterial infection. Conversely, transient overexpression of *dram1* promotes autophagic sequestration of mycobacteria and decreases mycobacterial infection [7]. In addition, human DRAM1 colocalizes with Mtb in infected macrophages [7]. Therefore, DRAM1 is a potential target for host directed therapy to restrict TB infection.

Macrophages commonly serve as the first innate immune cells to engulf mycobacteria and play a central role in TB pathogenesis [14, 15]. Nevertheless, mycobacteria can utilize macrophages as a niche in which they are able to survive and replicate via activation of diverse virulence mechanisms. For example, mycobacteria have evolved versatile mechanisms to alter the host environment, which prevents the delivery of mycobacteria to microbicidal lysosomes[16]. Arrested phagosome maturation or mycobacterial escape from phagosomes results in activation of autophagic defenses by infected macrophages [4, 17]. The role of autophagy in defense against mycobacterial infections has been studied well, both *in vitro* and *in vivo* [4, 7, 18]. The sequestering of an invading microbe by autophagy is called xenophagy [19]. In this process, selective autophagy receptors like p62, NDP52 and NBR1 serve as adaptor proteins to directly connect ubiquitin-tagged mycobacteria to forming autophagosomes [4, 20, 21]. Apart from directly capturing cytoplasmic mycobacteria by xenophagy, p62 also contributes to defense against mycobacteria by delivering ubiquitinated cytosolic proteins to autophagolysosomes, where they are proteolytically converted into neo-antimicrobial peptides [22]. Previously, our laboratory found that Dram1-mediated autophagic defense against mycobacterial infection requires the selective autophagy receptor p62 [7].

Intracellular proliferation of mycobacteria ultimately leads to the death of the macrophage that has phagocytosed them. The remains of this dead macrophage and the now extracellular bacteria will be engulfed by newly recruited macrophages, which themselves become infected and disseminate the infection [23]. However, the newly recruited macrophages phagocytose a large number of mycobacteria from the deceased macrophage, which means that newly infected macrophages will also die rapidly [24]. In general, once overproliferation of mycobacteria initiates death of individual macrophages, this will result in a cascade of infection and killing of newly recruited macrophages [25, 26]. Eventually, this leads to large scale dissemination of the infection and the formation of inflammatory infection foci, called granulomas [27, 28]. The granuloma is a compact and organized structure that is a typical pathological feature of TB disease [28, 29]. It is formed by mycobacteria-infected macrophages that attract other immune cells, like neutrophils, T cells, and B cells. On the one hand, granulomas function as host-protective structures to restrict mycobacteria locally [30]. However, these structures also provide a safe shelter for mycobacteria to persist inside the host for long periods and they are poorly penetrated by anti-mycobacterial drugs [31, 32]. Furthermore, recent studies have demonstrated that the process of granuloma formation facilitates the spreading of mycobacteria between macrophages and thereby promotes the dissemination of infection [23, 29, 33, 34]. Therefore, the fate of individual infected macrophages is a major determinant for the outcome of mycobacterial infection.

Mycobacteria-infected macrophages can undergo at least three general types of cell death: apoptosis, necrosis and pyroptosis[35]. Apoptosis is an energy-dependent form of programmed cell death that does not induce an inflammatory response upon execution [36, 37]. There are cell-extrinsic and -intrinsic pathways activating apoptosis, governed by the involvement of different initiator and effector cysteine-dependent aspartate-directed proteases (Caspases). The similarity between these two types of activation pathways is that both require the participation of Caspase 3 [38] The role of apoptotic macrophages in controlling mycobacterial infection has been well-established by *in vitro* studies [39, 40]. In contrast, recent *in vivo* studies have shown that mycobacteria-induced apoptosis tends to promote the spreading of the infection during early stages of granuloma formation in zebrafish [23, 41], although necrotic cell death of infected macrophages promotes the spreading of infection to an even greater extent [42]. Necrosis is

accompanied by swelling of organelles and damaging of the plasma membrane. This is generally considered a passive type of cell death but can also occur as a form of programmed cell death (necroptosis) [42, 43]. Eventually, released cytoplasmic material enters the extracellular space [37, 44]. Necrotic cell death of mycobacteria-infected macrophages facilitates dissemination of the infection and promotes granuloma formation both in zebrafish and mouse models [23, 45]. Pyroptotic cell death activates the inflammatory response during a process that requires the involvement of Caspase 1 [37, 38]. It is conceivable that pyroptosis, similar to other lytic types of cell death (necrosis, necroptosis), is beneficial to bacterial spreading and proliferation [46]. In summary, the fate of mycobacteria-infected macrophages plays an important role in TB pathogenesis. While a role for DRAM1 in autophagic defense against mycobacterial infections has been demonstrated [7], its potential function as a modulator of cell death during TB pathogenesis has not been explored.

In this study, we used zebrafish embryos and larvae infected with *Mycobacterium marinum* (Mm) as a model for TB pathogenesis to study the role of Dram1 in controlling mycobacterial infection. We have generated two zebrafish *dram1* mutant alleles using CRISPR/Cas9-mediated mutagenesis. Using these mutants, we have demonstrated that Dram1 deficiency has no apparent effect on development and does not reduce basal levels of autophagy in zebrafish larvae under non-infected conditions. Confirming and extending our previous knockdown studies, we present evidence that Dram1 is required for autophagic targeting and host defense against Mm. Specifically, analysis of the mutant fish showed that Dram1 is required for maturation of Mm-containing vesicles and for macrophages to restrict Mm infection. Without functional Dram1, Mm-infected macrophages initiate programmed cell death via a Caspase 1-dependent mechanism, indicative of pyroptosis. Collectively, our data advocate that Dram1 protects against mycobacterial infection by modulating autophagic targeting and maturation of Mm-containing vesicles. In the absence of Dram1, infected macrophages rapidly become overburdened by the bacteria and initiate pyroptotic cell death, resulting in increased dissemination of the infection.

Results

Generation of Dram1 null mutants by CRISPR/Cas9 method

In a previous study, we have shown that the autophagy modulator Dram1 protects against mycobacterial infection via stimulation of autophagic defenses and maturation of bacteria-containing vesicles [7]. Here, we generated a zebrafish *dram1* mutant line using CRISPR/Cas9 technology to validate and expand on our previous findings. We designed a single guide RNA (sgRNA) that targets the CRISPR/Cas9 endonuclease complex to the first coding exon of the *dram1* gene (Fig1 A). We predicted that random insertions or deletions around the target site due to non-homologous end joining would introduce a frame shift and/or premature stop codon, ensuring that the Dram1 protein will not be translated (Fig1 A). We injected the sgRNA and Cas9 mRNA into the yolk of one cell stage embryos and analyzed the resulting mutations by Sanger sequencing to identify F0 founders (FigS1 A). Dram1 is known as a modulator of autophagy [11]. Thus, F0 founders carrying two independent mutations in exon1 of *dram1* were outcrossed with *Tg*(*CMV:EGFP-map1lc3b*) fish (hereafter referred to a GFP-Lc3) to allow visualization of autophagic processes [47]. Upon adulthood, F1 heterozygous carriers of the mutated *dram1* alleles ($dram1^{+/-}$) were incrossed to obtain F2 homozygous mutants ($dram1^{-/-}$) and wild type siblings ($dram1^{+/+}$) with or without GFP-Lc3 in the background. We performed Sanger sequencing on genomic DNA (F2) obtained from fin tissue to characterize the two independent mutant alleles: 1) a 21 nucleotides deletion combined with a 2 nucleotides insertion at the target site, named $dram1^{\Delta 19n/\Delta 19n}$ (Fig1 B); and 2) a 5 nucleotides insertion at the target site, named $dram1^{5n/5n}$ (FigS1 B). In this study, we focused primarily on the $dram1^{\Delta 19n/\Delta 19n}$ allele, and confirmed crucial observations with the $dram1^{5n/5n}$ allele. Using an N-terminal antibody capable of detecting zebrafish Dram1 by western blot, we could not detect Dram1 protein in the $dram1^{\Delta 19n/\Delta 19n}$ line, supporting that this represents a null allele (Fig1 C).

Apart from its important role in autophagy, Dram1 has also been found to modulate other cellular processes, including apoptosis and neutrophil differentiation[11, 48]. We therefore first asked whether Dram1 deficiency results in developmental defects. We compared body size measurements, but found no apparent difference in development between $dram1^{\Delta 19n/\Delta 19n}$ and

wild type siblings (*dram1*$^{+/+}$) (Fig1 E). Furthermore, *dram1*$^{\Delta 19n/\Delta 19n}$ larvae or adult fish (up to 18 months) did not exhibit observable differences in behavior, survival, or fertility compared to *dram1*$^{+/+}$ (data not shown). Finally, we used a Chi-square test to determine that the offspring from incrossed heterozygous *dram1*$^{\Delta 19N}$ (hereafter referred to as *dram1*$^{\Delta 19n/+}$) strictly followed Mendelian inheritance (Fig1 D). The same was true for incrossed *dram1*$^{5n/+}$ parents (FigS1 C). We also performed Tunel staining to detect if Dram1 deficiency affect the basal cell death, the result showed that *dram1*$^{+/+}$ and *dram1*$^{\Delta 19n/\Delta 19n}$ display similar numbers of Tunel^{+} cells (Fig1 F and G). Collectively, we have used CRISPR/Cas9 targeted mutagenesis to generate two *dram1* null mutants, both of which display no apparent phenotypes during development and can be used to study the function of Dram1 in autophagy and immune defense against infection.

Figure 1: Generation of Dram1 mutant lines (Figure on next page)

A. Schematic representation of the zebrafish *dram1*/Dram1(ENSDARG00000045561/ENSDARP0 0000066996.3) genetic and protein domain architecture and CRISPR/Cas9 target site. Dram1 (240 amino acids) contains six transmembrane domains, which are indicated with grey boxes and labels (T1-T6) with amino acid numbers above. The gene is depicted with coding exons as grey boxes and introns as solid black lines (introns not drawn to scale). The position of the CRISPR/Cas9 target site at the beginning of the first coding exon is indicated and the predicted truncated protein in the *dram1*$^{\Delta 19n/\Delta 19n}$ mutant line is drawn above. The *dram1*$^{5n/5n}$ allele was generated at the same target site, leading to a similarly truncated protein (FigS1).

B. Sanger sequencing of *dram1*$^{\Delta 19n/\Delta 19n}$ and *dram1*$^{+/+}$ from F2 offspring. Red lines indicate CRISPR/Cas9 target sites. The genomic DNA was isolated from fin tissue (>3 months old fish). The *dram1*$^{\Delta 19n/\Delta 19n}$ mutant allele has 21 nucleotides deleted and 2 nucleotides inserted.

C. Confirmation of truncation of the Dram1 protein by western blotting analysis. Protein samples were extracted from 4 dpf *dram1*$^{\Delta 19n/\Delta 19n}$ and *dram1*$^{+/+}$ larvae (>10 larvae/sample). The blots were probed with antibodies against Dram1 and Actin as a loading control.

D. Segregation from *dram1*$^{\Delta 19n/+}$ F1 heterozygous incross. Genotypes of adult fish (>3 months old) were combined from at least three independent breedings and confirmed by PCR and Sanger sequencing. Data were analyzed by Chi Square test. ns, non-significant,*p<0.05,**p<0.01,***p<0.001.

E. Measurements of larval body lengths. *dram1*$^{+/+}$ and *dram1*$^{\Delta 19n/\Delta 19n}$ larvae (≥10 larvae/group) were imaged by stereo microscopy at 3dpf and body lengths were measured as indicated by the red dotted lines.

F. Basal cell death was detected in *dram1*$^{\Delta 19n/\Delta 19n}$ and *dram1*$^{+/+}$ larvae in the tail region. Tunel staining was performed on 3 dpf larvae to detect cell death (≥7 larvae/group). ns, non-significant, *p<0.05, **p<0.01, ***p<0.001

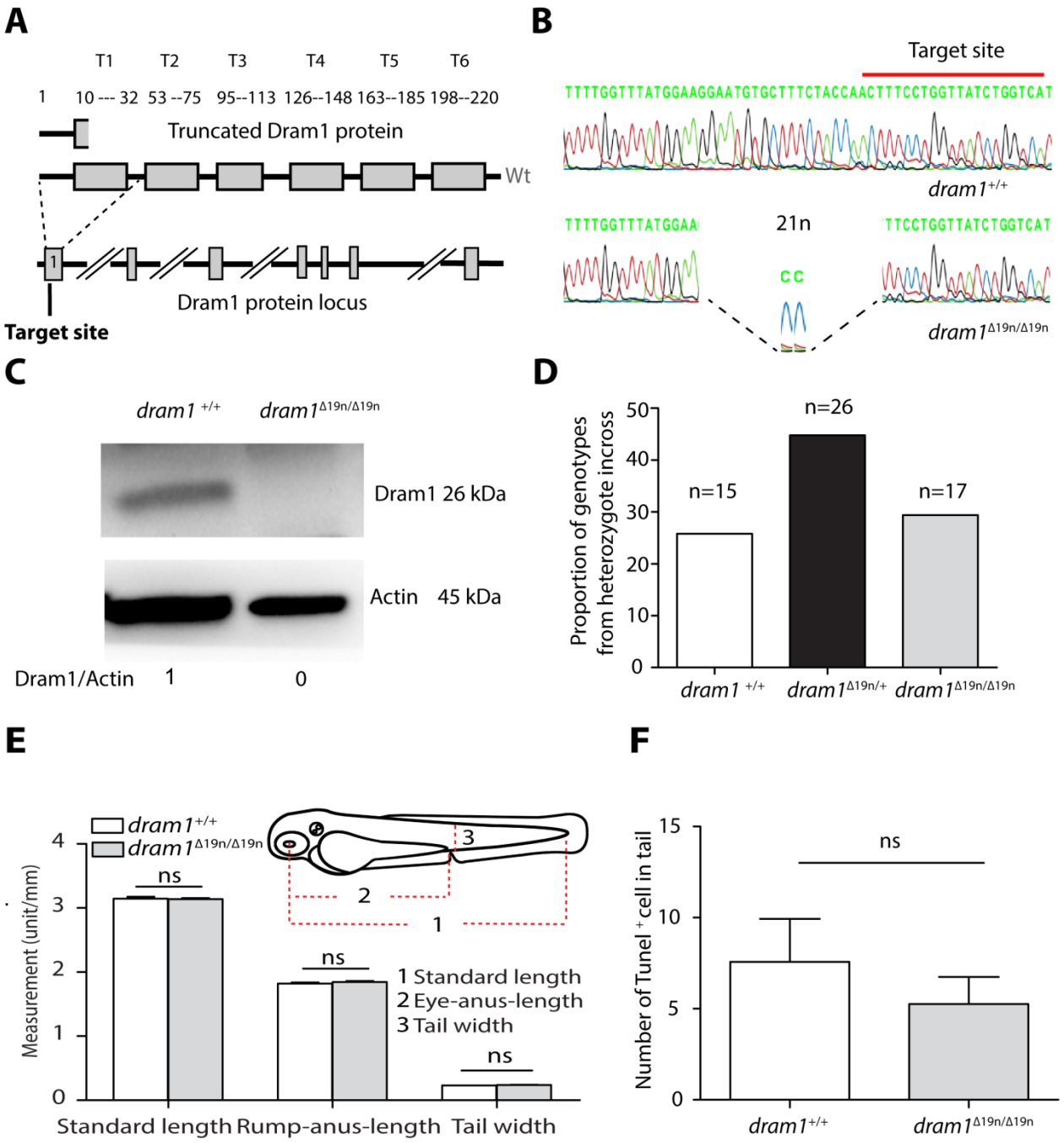

dram1 null mutants display increased susceptibility to mycobacterial infection

Since transient knockdown of zebrafish *dram1* by antisense morpholino oligonucleotide knockdown resulted in increased Mm infection and extracellular growth of bacteria [7], we sought

to confirm this phenotype in our *dram1* mutants. Therefore, we infected *dram1*$^{\Delta 19n/\Delta 19n}$, *dram1*$^{+/+}$, and unrelated wild types (AB/TL) with Mm at 1 dpf via blood island injection and found that *dram1*$^{\Delta 19n/\Delta 19n}$ had a significantly increased susceptibility to infection (Fig2 A and B). Furthermore, Dram1-deficient larvae randomly displayed accumulation of bacteria inside intersegmental blood vessels at 3 days post infection (dpi), which is indicative of extracellular growth of bacteria (Fig2 A). We detected no differences in bacterial burden between *dram*$^{+/+}$ and unrelated wild types, indicating that the genetic background in which the mutation was made did not affect its susceptibility to mycobacterial infection (Fig2 B). Mycobacterial infection in *dram1*$^{\Delta 19n/\Delta 19n}$ resulted in a clearly increased infection burden of around 290% compared to their WT siblings (Fig2 B). We next tested the infection susceptibility of larvae homozygous for the other *dram1* mutant allele, *dram1*$^{5n/5n}$, and found that it roughly exhibited the same increase (around 250%) compared to their wild type siblings (FigS2 B and FigS2 C). As expected, these experiments demonstrated that both *dram1* mutant alleles (19n indel and 5n indel) were more susceptible to mycobacterial infection. Since there are no clear differences between the two mutant alleles in susceptibility to Mm infection, we decided to use the *dram1*$^{\Delta 19n/\Delta 19n}$ allele for further study into Dram1 function.

Next, we asked if transient overexpression of *dram1* mRNA can compensate for Dram1-deficiency in *dram1*$^{\Delta 19n/\Delta 19n}$. For this purpose, we injected *dram1* mRNA into one cell *dram1*$^{\Delta 19n/\Delta 19n}$ and *dram*$^{+/+}$ embryos to overexpress *dram1*. As a negative control, we also injected *dram1* mutant mRNA, which was generated from cDNA obtained from *dram1*$^{\Delta 19n/\Delta 19n}$. The results showed that transient overexpression of *dram1* mRNA rescued Dram1 deficiency during mycobacterial infection, while overexpression of mutant *dram1* mRNA did not affect Mm infection burden (Fig2 C). Collectively, our analysis of two zebrafish *dram1* mutant alleles confirms that Dram1 is necessary for host defense during Mm infection.

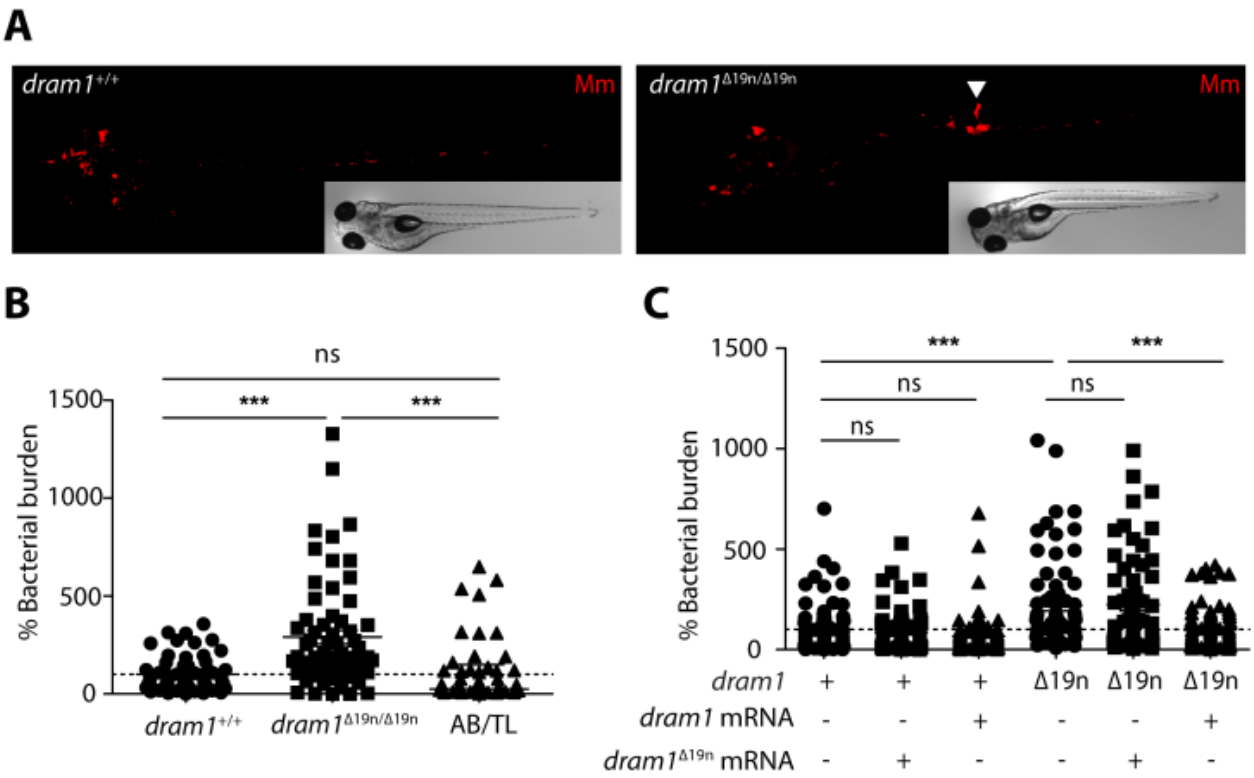

Figure 2: Dram1 deficiency leads to increased susceptibility to Mm infection

A. Representative stereo images of infected *dram1*$^{\Delta 19n/\Delta 19n}$ and *dram1*$^{+/+}$ larvae at 3 dpi**.**

B. Bacterial burdens were determined at 3dpi. The data is accumulated from two independent infection experiments. Each dot represents an individual larva. The arrowhead indicates the accumulation of bacteria in intersegmental veins. ns, non-significant, *p<0.05,**p<0.01,***p<0.001 .

C. Embryos were injected at the one cell stage with 50 ng of *dram1* or *dram1*$^{\Delta 19n}$ mRNA, or non injected. Data is accumulated from two independent infection experiments. Each dot represents an individual larva. ns, non-significant, *p<0.05,**p<0.01,***p<0.001.

Analyzing autophagic processes in *dram1* null mutants suggests defects in autophagosome maturation

Human DRAM1 is a modulator of autophagy and DRAM1 deficiency results in impaired autophagy induction *in vitro*[11]. Furthermore, a role for DRAM1 in maturation of autophagosomes has been described [49]. Therefore, we assessed the effect of zebrafish dram1 mutation on autophagy in developing embryos (Fig3 A). Increased GFP-Lc3 puncta and LC3-II protein levels can indicate enhanced autophagosome formation [50]. However, increased GFP-Lc3

puncta or Lc3-II protein levels can also indicate a block in degradation of autophagosomes (reduced autophagic flux). First, we used the GFP-Lc3 reporter to analyze whether differences in basal autophagy could be detected due to Dram1 deficiency. We imaged GFP-Lc3 puncta in the tail fin tissue of *dram1*$^{\Delta 19n/\Delta 19n}$ and *dram1*$^{+/+}$. Although the average number of autophagy-related structures was slightly higher in *dram1*$^{\Delta 19n/\Delta 19n}$, the difference between the two groups under basal conditions was not significant (Fig3 B). However, there might be differences that are obscured by ongoing autophagic flux, or that only become apparent under certain conditions. Therefore, we examined GFP-Lc3 accumulation following treatment with the vacuolar H+ ATPase (V-ATPase) inhibitor Bafilomycin A1 (BafA1). Treatment with BafA1 prevents maturation of autophagic vacuoles by inhibiting fusion between autophagosomes and lysosomes [51, 52]. While BafA1 treatment resulted in accumulation of GFP-Lc3 puncta in both *dram1*$^{\Delta 19n/\Delta 19n}$ and *dram1*$^{+/+}$, the dram1 mutants accumulated more GFP-Lc3 puncta than their wild type siblings (Fig3 C). To independently confirm these results, we next detected endogenous Lc3 protein levels by western blot. In agreement with the GFP-Lc3 puncta analysis, Lc3-II protein levels were not detectably different between *dram1*$^{\Delta 19n/\Delta 19n}$ and *dram1*$^{+/+}$ larvae under basal conditions, but Dram1 deficiency significantly increased Lc3-II protein levels when autophagic flux is blocked by BafA1 treatment (Fig3 D and E). Finally, we assessed the protein levels of p62 and Optineurin, since these ubiquitin-binding receptors are depleted during selective autophagy [53-55]. Therefore, protein levels of p62, as well as Optineurin, can be used as an inverse indicator of autophagy activity [56]. The results showed that Optineurin and p62 protein levels were similar in *dram1*$^{\Delta 19n/\Delta 19n}$ and *dram1*$^{+/+}$ under basal conditions but were elevated in *dram1*$^{\Delta 19n/\Delta 19n}$ larvae when autophagic flux is blocked in the presence of BafA1 (FigS3 A). This accumulation of Optineurin and p62 could be due either to increased production or to reduced degradation of these selective autophagy receptors. Taken together, Dram1 deficiency did not cause detectable differences in autophagic processes under basal conditions. However, blocking autophagic flux revealed alterations in the autophagy pathway that could be explained by an increase in autophagosome formation, a defect in autophagosome maturation, or both.

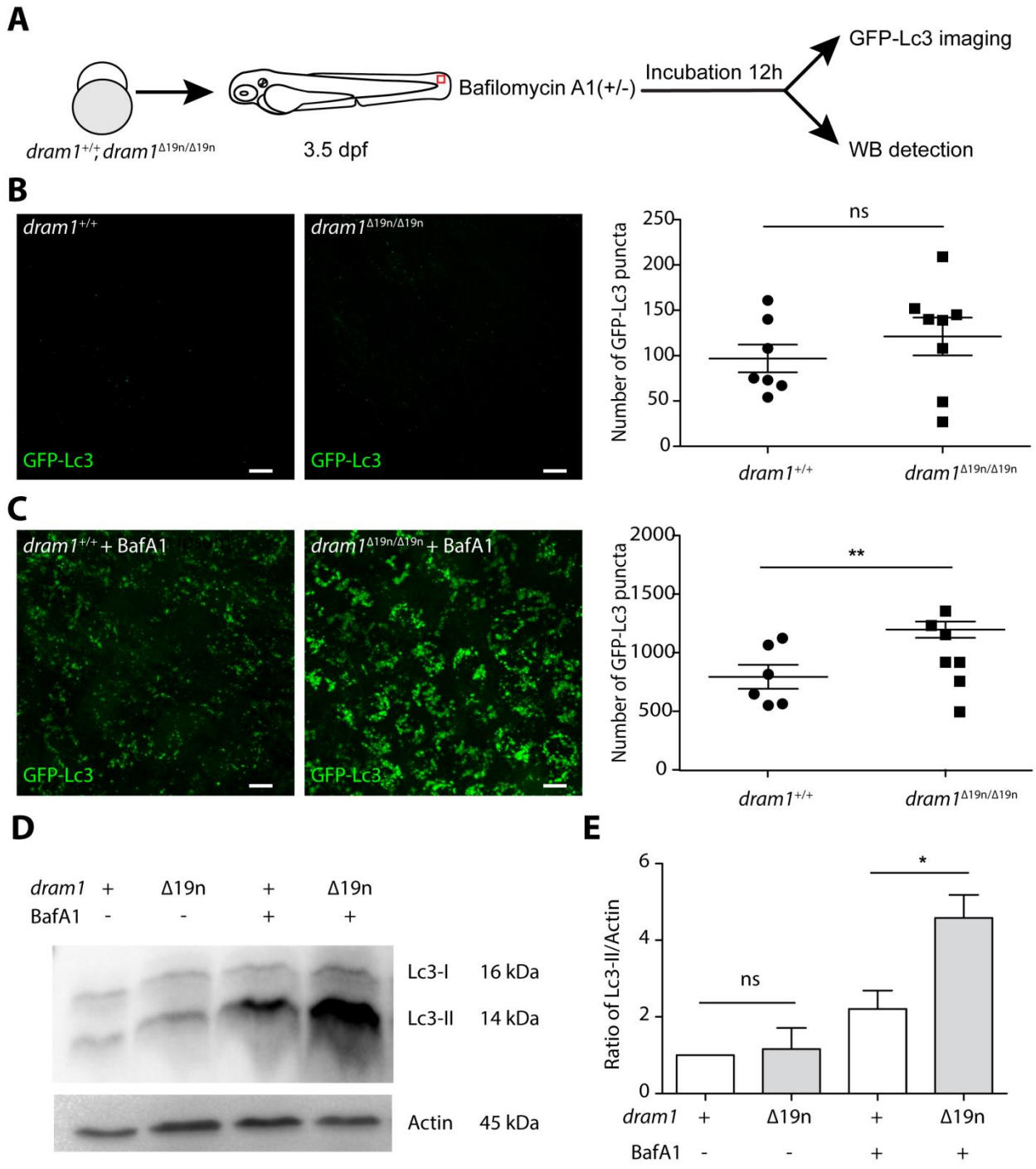

Figure 3: Dram1 mutation leads to impairment in autophagic flux

A. Workflow representing the experimental design followed in panels B-D. 3.5 dpf larvae were treated with BafA1 (100 nM) for 12h or no treatment. The *dram1*$^{\Delta 19n/\Delta 19n}$ and *dram1*$^{+/+}$ larvae in GFP-Lc3 background were used for

monitoring autophagic activity using confocal imaging. The *dram1*$^{\Delta 19n/\Delta 19n}$ and *dram1*$^{+/+}$ larvae not carrying GFP-Lc3 were used for assaying autophagy activity by western blot (WB).

B-C. Representative confocal micrographs of GFP-Lc3 puncta present in the tail fin, and quantification of the number of GFP-Lc3 puncta in *dram1*$^{\Delta 19n/\Delta 19n}$ and *dram1*$^{+/+}$ larvae in an unstimulated situation (basal autophagy, B) and following BafA1 treatment (C). Each larva was imaged at a pre-defined region of the tail fin (as indicated by the red boxed area in Fig3 A) (≥6 larvae/group). Results are representative of two independent experiments. Scale bars, 10 μm.

D. Lc3 protein levels were detected in *dram1*$^{\Delta 19n/\Delta 19n}$ and *dram1*$^{+/+}$ larvae in absence or presence of BafA1. Protein samples were obtained from 4 dpf *dram1*$^{\Delta 19n/\Delta 19n}$ and *dram1*$^{+/+}$ larvae (>10 larvae/sample). The WB were probed with antibodies against Lc3 and Actin as a loading control. WB were repeated three times with protein extracts derived from independent experiments.

E. Lc3-II/Actin ratios were quantified from the blots of *dram1*$^{\Delta 19n/\Delta 19n}$ and *dram1*$^{+/+}$ larvae in absence or presence of BafA1. WB band intensities were quantified by Lab Image (Bio-Rad). The data were combined from three independent experiments.

Dram1 deficiency leads to reduced GFP-Lc3 targeting of mycobacteria, but accumulated Lc3-II protein levels

We previously found that Dram1 mediates autophagic defense against Mm and that *dram1* knockdown decreased targeting of autophagic vesicles to Mm [7]. Thus, we infected *dram1*$^{\Delta 19n/\Delta 19n}$ and *dram1*$^{+/+}$ in a GFP-Lc3 background with Mm to determine whether *dram1* knockout confirms our previous observations. We used confocal laser scanning microscopy to image the entire caudal hematopoietic tissue (CHT) at 2 dpi, since the majority of immune cells that have phagocytosed Mm are present in the CHT at this time point (Fig4 A). We quantified the colocalization between GFP-Lc3 and Mm and found that *dram1*$^{\Delta 19n/\Delta 19n}$ larvae displayed significantly less GFP-Lc3-positive Mm clusters compared to their wild type siblings (Fig4 B). Approximately 9% of the Mm clusters were positive for GFP-Lc3 in wild type siblings, opposed to only around 3% in *dram1*$^{\Delta 19n/\Delta 19n}$ (Fig4 C). Since Dram1 deficiency reduced autophagic targeting of Mm, we expected to detect lower Lc3-II protein levels by western blot at 3 dpi. The results showed that Mm infection increased Lc3-II levels in *dram1*$^{\Delta 19n/\Delta 19n}$ and *dram1*$^{+/+}$ (Fig4 D), consistent with the observed autophagic targeting of Mm (Fig4 B). However, the results also showed that Dram1-deficient larvae accumulated more Lc3-II than their wild type siblings during

Mm infection (Fig4 D), which was opposite to our expectation. Since ubiquitination of cytoplasmic cargo plays an important role in selective autophagy against mycobacteria [20], we performed western blot detection of ubiquitinated proteins on non-infected and infected *dram1*$^{\Delta 19n/\Delta 19n}$ and *dram1*$^{+/+}$. The results showed that Dram1 deficiency led to accumulation of ubiquitinated proteins during the infection (FigS4 A). In conclusion, Mm infection results in increased accumulation of Lc3-II and ubiquitinated proteins. While these proteins accumulate at even higher levels in Dram1-deficient larvae, we clearly observed reduced autophagic targeting of Mm in the absence of Dram1.

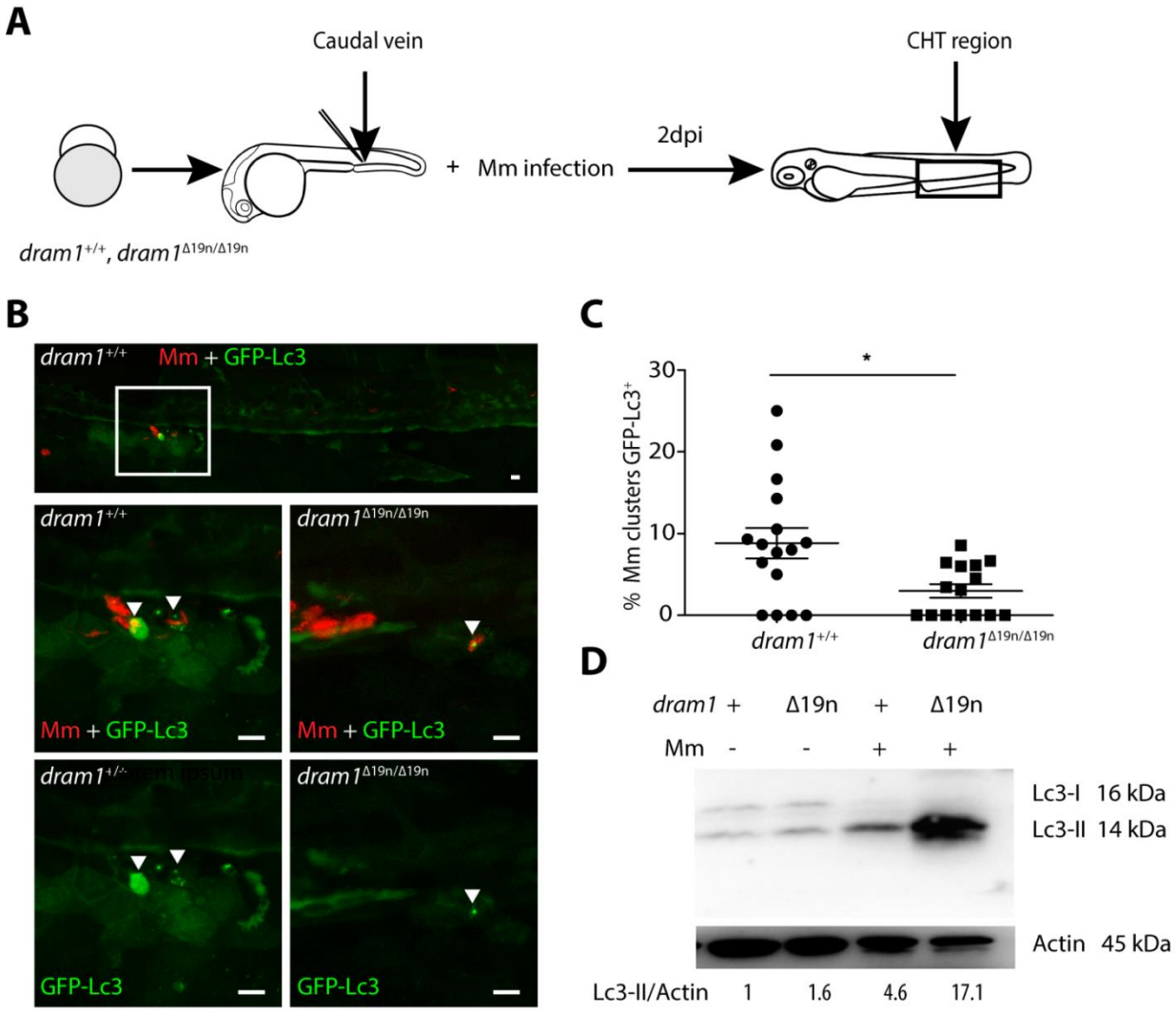

Figure 4: Dram1 is required for GFP-Lc3 targeting to Mm clusters

A. Workflow representing the experimental design followed in B. 2 dpi fixed larvae were used for confocal imaging. The entire caudal hematopoietic tissue (CHT) was imaged, as indicated by the black box.

B. Representative confocal micrographs of GFP-Lc3 co-localization with Mm clusters in infected *dram1*$^{\Delta 19n/\Delta 19n}$ and *dram1*$^{+/+}$ larvae. The top image shows the entire CHT region. the bottom images show GFP-Lc3 colocalization of Mm clusters in *dram1*$^{\Delta 19n/\Delta 19n}$ and *dram1*$^{+/+}$ larvae. The arrowheads indicate the overlap between GFP-Lc3 and Mm clusters. Scale bars, 10 μm.

C. Quantification of the percentage of Mm clusters positive for GFP-Lc3 vesicles. The data is accumulated from two independent experiments, each dot represents an individual larva (≥15 larvae/group).

D. Lc3 protein levels were determined by WB in infected and uninfected larvae. Protein samples were extracted from 4 dpf larvae (>10 larvae/sample). The blots were probed with antibodies against Lc3 and Actin as a loading control. WBs were repeated two times with independent extracts.

Dram1-deficiency does not affect phagocytosis of Mm

Macrophages play an important role in defense against mycobacterial infections. Thus, we were interested to know whether Dram1 deficiency affects the immune functions of macrophages. Therefore, the *dram1*$^{\Delta 19n/\Delta 19n}$ line was outcrossed with the macrophage marker line *Tg*(*mpeg1:mCherry-F*)^{umsF001} [57] and subsequently incrossed to obtain *dram1*$^{+/+}$, *dram1*$^{\Delta 19n/+}$, and *dram1*$^{\Delta 19n/\Delta 19n}$ with an *mpeg1*-driven and membrane-localizing *mCherry-F* in the background (FigS1 A and D). Since human DRAM1 is involved in cellular differentiation of immune cells [48], we first asked whether Dram1-deficiency affected the development of immune cells in zebrafish. For this purpose, we performed TSA-staining to count the number of neutrophils and utilized the *mpeg1:mCherry-F* reporter to count the number of macrophages. The results revealed that Dram1 deficiency did not alter the number of macrophages and neutrophils (Fig5 A and Fig5 B). Since the first stages of TB pathogenesis take place inside macrophages, we asked whether increased mycobacterial burden caused by Dram1 deficiency was due to defects in phagocytosis by macrophages. We infected *dram1*$^{\Delta 19n/\Delta 19n}$ and *dram1*$^{+/+}$ with Mm and assessed the phagocytic activity of leukocytes at 1 hour post infection (hpi). The results showed that Mm were phagocytosed by macrophages both in *dram1*$^{\Delta 19n/\Delta 19n}$ and their wild type siblings, and there was no significant difference in the percentage of Mm clusters that reside inside macrophages at 1 hpi (Fig5 C and Fig5 D). Next, we determined at which time point during the infection we were

first able to detect a difference in bacterial burden between *dram1*$^{\Delta 19n/\Delta 19n}$ and *dram1*$^{+/+}$. We found that there was no detectable difference in Mm infection burden at 1 dpi, but Dram1 deficiency significantly increased Mm infection burden at 2 dpi (Fig5 E and Fig5 F). In conclusion, Mm are phagocytosed at a similar rate by *dram1*$^{\Delta 19n/\Delta 19n}$ and *dram1*$^{+/+}$, and the immunocompromised state of Dram1-deficient larvae first becomes apparent at 2 days post infection.

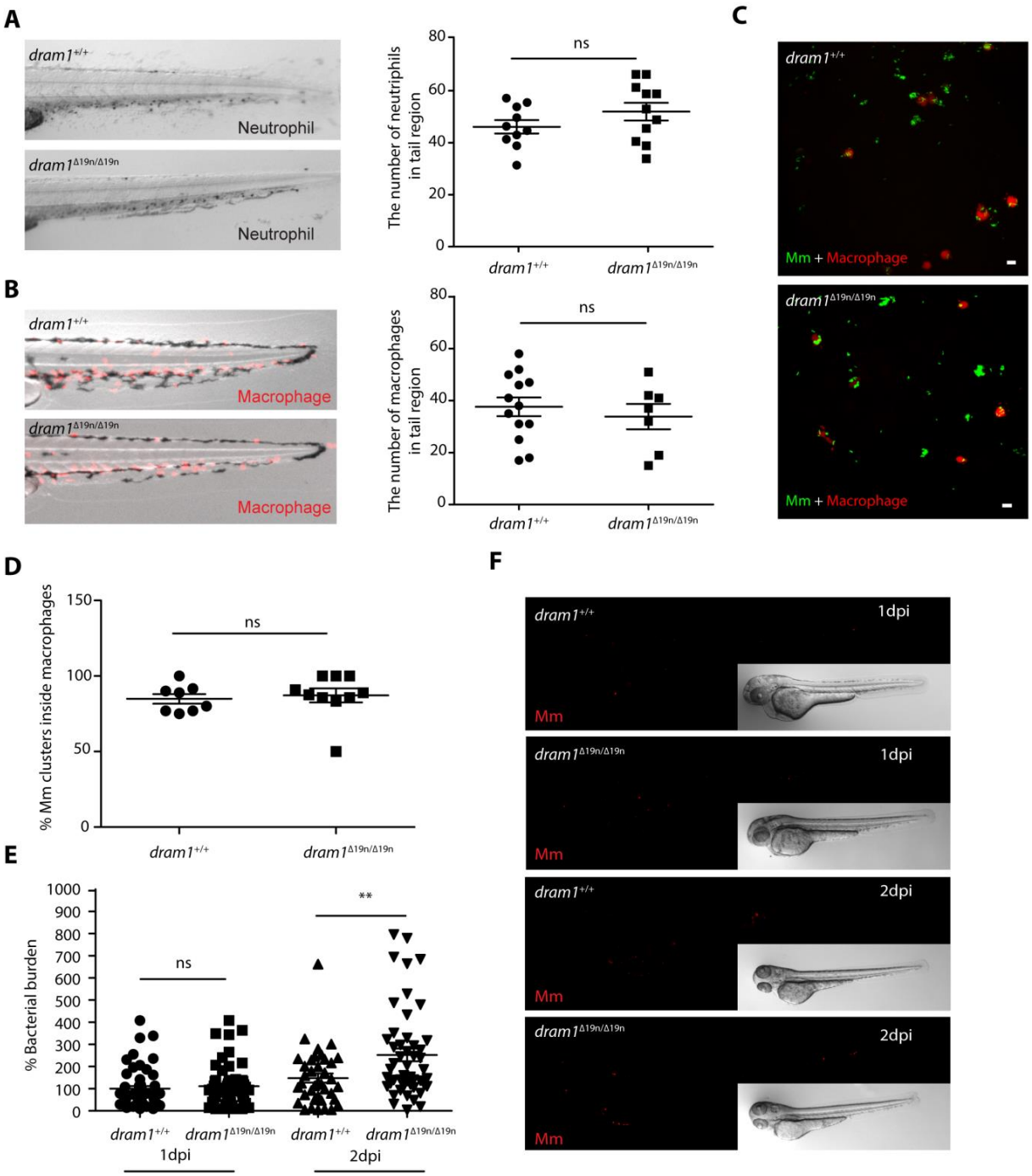

Figure 5: Dram1 deficiency does not affect the capability of macrophages to phagocytose Mm

A. Representative stereo images of the whole tail of *dram1*$^{\Delta 19n/\Delta 19n}$ and *dram1*$^{+/+}$ larvae following an immunohistochemical peroxidase activity detection protocol. The number of neutrophils in this region was quantified per individual larva (≥10 larvae/group). Each data point represents an individual larva. The results are representative for two individual repeats.

B. Representative stereo micrographs of macrophages in the whole tail region and quantification of the number of macrophages in this region. 3 dpf *dram1*$^{\Delta 19n/\Delta 19n}$ and *dram1*$^{+/+}$/ *mpeg1:mCherry-F* larvae were obtained from incrossed *dram1*$^{\Delta 19n/+}$ animals and the number of macrophages for each larva were counted before knowing the genotype. Genotyping was performed by PCR and Sanger sequencing (≥7 larvae/ group). The results are representative for two individual repeats.

C. Representative confocal micrographs of the yolk of infected *dram1*$^{\Delta 19n/\Delta 19n}$ and *dram1*$^{+/+}$ embryos in *mpeg1:mCherry-F* background at 1 hour post infection (hpi). Scale bars, 10 µm.

D. Quantification of phagocytosis of Mm by macrophages at 1 hpi. *dram1*$^{\Delta 19n/\Delta 19n}$ and *dram1*$^{+/+}$ embryos in *mpeg1:mCherry-F* background were infected Mm at 30 hpf and fixed at 1 hpi. Each dot represents the percentage of macrophages that have phagocytosed Mm clusters in an individual larva (≥8 larvae/ group). The results are representative for two individual repeats.

E. Bacterial pixel counts were determined at 1 and 2 dpi for infected embryos. *dram1*$^{\Delta 19n/\Delta 19n}$ and *dram1*$^{+/+}$. Each dot represents an individual infected larva. ns, non-significant, *p<0.05,**p<0.01,***p<0.001 ..

F. Representative stereo images of infected *dram1*$^{\Delta 19n/\Delta 19n}$ and *dram1*$^{+/+}$ embryos at 1 and 2 dpi.

Dram1 is required for macrophages to restrict Mm infection

Since Dram1 is a lysosomal membrane protein [11], we asked whether Dram1-deficiency affected the maturation of Mm-containing vesicles. We used LysoTracker to determine the extent of colocalization between Mm and acidic vesicles in the CHT at 1 dpi, a time point at which we did not observe a difference in bacterial burden between *dram1*$^{\Delta 19n/\Delta 19n}$ and *dram1*$^{+/+}$ yet (Fig5 E). In wild type siblings, we observed that roughly 60% of the bacterial clusters were LysoTracker-positive, while in Dram1-deficient larvae only roughly 20% of the bacterial clusters were positive for LysoTracker staining (Fig6 B). This implicates that Dram1 is indeed required for maturation of Mm-containing vesicles. Next, we asked whether the reduced maturation of Mm-containing vesicles limits the ability of macrophages in *dram1*$^{\Delta 19n/\Delta 19n}$ hosts to combat the infection. The results showed that at 1 dpi the majority of Mm clusters were restricted inside macrophages both in *dram1*$^{\Delta 19n/\Delta 19n}$ and *dram1*$^{+/+}$ (63% and 75%, respectively; Fig6 C and Fig6 D). However, at

2 dpi, we observed that the majority of Mm remained inside of macrophages in *dram1*$^{+/+}$ (65%), while in *dram1*$^{\Delta 19n/\Delta 19n}$ larvae we found that most Mm had escaped from macrophages and only 31% remained intracellular (Fig6 E and F). Furthermore, we frequently observed evidence of macrophage cell death in the proximity of bacterial clusters in *dram1*$^{\Delta 19n/\Delta 19n}$ (Fig6 E). Together, these data demonstrated that Dram1 is necessary for macrophages to restrict mycobacterial infection and prevent extracellular growth of the bacteria.

Figure 6: Macrophages fail to restrict Mm infection in Dram1-deficient larvae (Figure on next page)

A. Representative confocal images of LysoTracker staining performed on *dram1*$^{\Delta 19n/\Delta 19n}$ and *dram1*$^{+/+}$ embryos at 1 dpi. The arrowheads indicate the colocalization between Mm and LysoTracker staining. Scale bars, 10 µm.

B. The percentage of Mm clusters positive for LysoTracker staining (LysoTracker^{+}) was determined in infected embryos (≥10 embryos/group) at 1 dpi. Each dot represents the percentage of Mm clusters that are LysoTracker^{+} in an individual infected larva. Data is representative of two independent experiments. ns, non-significant,*p<0.05,**p<0.01,***p<0.001.

C and D Representative confocal images of *dram1*$^{\Delta 19n/\Delta 19n}$ and *dram1*$^{+/+}$ embryos/larvae in *mpeg1:mCherry-F* background, infected as described in Fig6 A, at 1 and 2 dpi. The entire CHT region of fixed embryos or larvae was imaged. The arrowheads indicate extracellular Mm clusters and stars(*) indicate dead macrophages. Scale bars, 10 µm.

E and F: The percentage of Mm clusters restricted inside macrophages was determined at 1 and 2 dpi (≥5 embryos/group). Each dot represents the percentage of intracellular Mm clusters in an individual embryos. Data is representative of two independent experiments. ns, non-significant,*p<0.05,**p<0.01,***p<0.001.

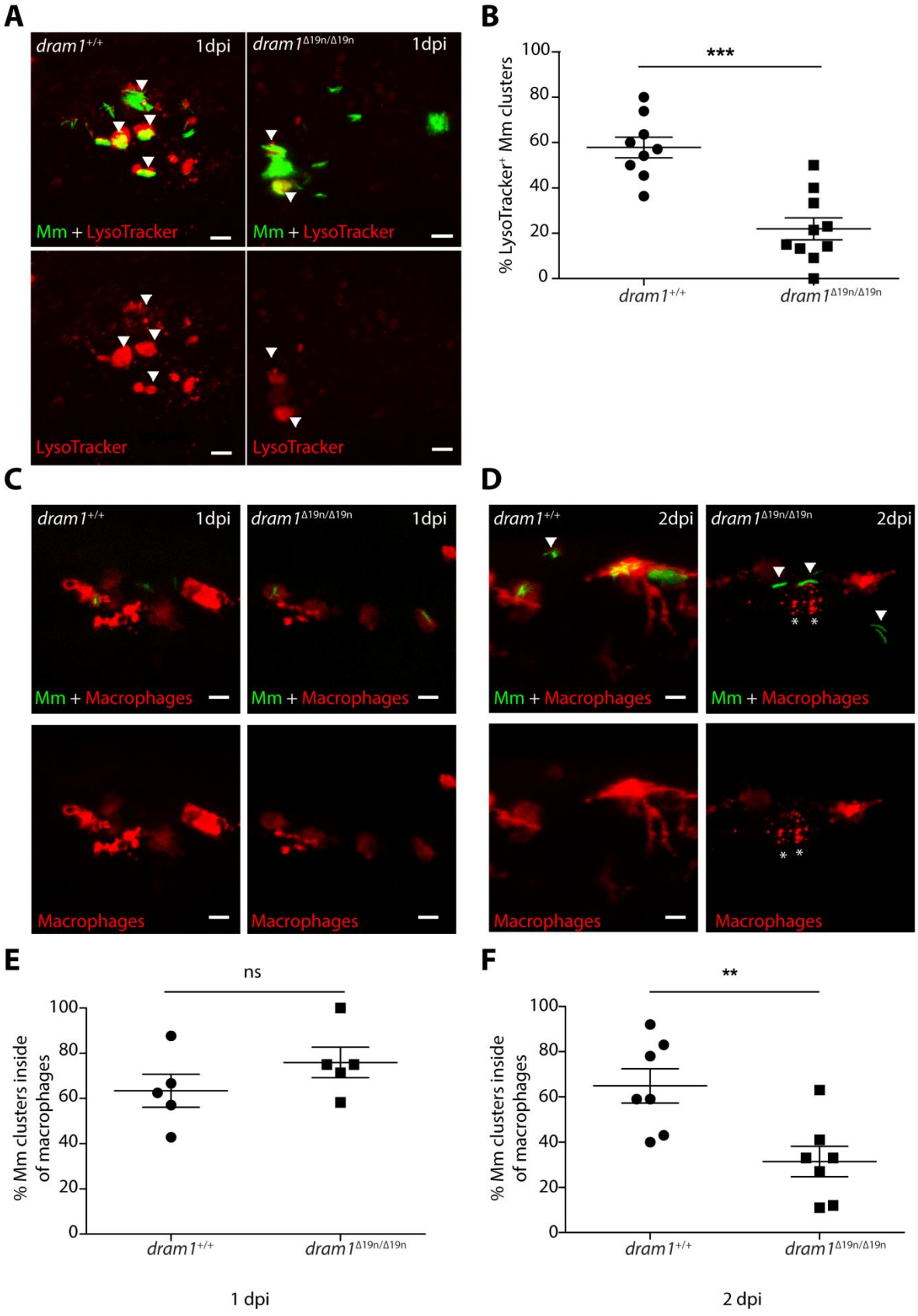
A
dram1+/+
1dpi
dram1Δ19n/Δ19n
1dpi
Mm + LysoTracker
Mm + LysoTracker
LysoTracker
LysoTracker
B
% LysoTracker+ Mm clusters
100
80
60
40
20
0
***
dram1+/+
dram1Δ19n/Δ19n
C
dram1+/+
1dpi
dram1Δ19n/Δ19n
1dpi
Mm + Macrophages
Mm + Macrophages
Macrophages
Macrophages
D
dram1+/+
2dpi
dram1Δ19n/Δ19n
2dpi
Mm + Macrophages
Mm + Macrophages
Macrophages
Macrophages
E
% Mm clusters inside of macrophages
100
80
60
40
20
0
ns
dram1+/+
dram1Δ19n/Δ19n
1 dpi
F
% Mm clusters inside of macrophages
100
80
60
40
20
0
**
dram1+/+
dram1Δ19n/Δ19n
2 dpi

Dram1 deficiency results in increased Caspase-1 dependent programmed cell death

Since we observed many dead macrophages around Mm in *dram1*$^{\Delta 19n/\Delta 19n}$ at 2 and 3 dpi (Fig6 E and data not shown), we aimed to decipher the mechanism responsible for this cell death. Thus, we performed Terminal deoxynucleotidyl transferase dUTP nick end labeling (Tunel) on infected embryos and imaged the entire CHT region of *dram1*$^{\Delta 19n/\Delta 19n}$ and *dram1*$^{+/+}$. This staining can detect damaged DNA present both in apoptotic and pyroptotic cells [58, 59]. We could observe Tunel-positive cells around Mm clusters both in *dram1*$^{\Delta 19n/\Delta 19n}$ and *dram1*$^{+/+}$ (Fig7 A). The results showed that the percentage of Tunel-positive Mm clusters was around 2.1 times higher in *dram1*$^{\Delta 19n/\Delta 19n}$ when compared to *dram1*$^{+/+}$ (Fig7 B). Human DRAM1 has previously been reported as a regulator of apoptosis [12]. Thus, we determined whether Dram1-deficiency affected apoptosis in response to infection. Caspase 3 serves as a main executioner and indicator of apoptotic cell death [38, 60]. We therefore utilized an antibody against full length and active Caspase 3 to monitor apoptosis activity by western blot in *dram1*$^{\Delta 19n/\Delta 19n}$ and *dram1*$^{+/+}$. The results showed that Caspase 3 was activated (cleaved) in response to Mm infection in *dram1*$^{\Delta 19n/\Delta 19n}$ and *dram1*$^{+/+}$. However, we did not detect any difference in the levels of Caspase 3 activation between *dram1*$^{\Delta 19n/\Delta 19n}$ and *dram1*$^{+/+}$ (Fig7 C). This indicated that cells undergo apoptosis in *dram1*$^{\Delta 19n/\Delta 19n}$ and *dram1*$^{+/+}$ during Mm infection but did not provide evidence that the increased cell death observed in *dram1*$^{\Delta 19n/\Delta 19n}$ was due to increased apoptosis. Next, we asked if these macrophages died via pyroptotic cell death. Pyroptosis is a Caspase 1-dependent form of cell death [37]. Thus, we detected Caspase 1 activity in the absence and presence of Mm infection in *dram1*$^{\Delta 19n/\Delta 19n}$ and *dram1*$^{+/+}$ at 2dpf, the time point at which we observed increased cell death in *dram1*$^{\Delta 19n/\Delta 19n}$. The results showed that Caspase 1 activity was increased in *dram1*$^{\Delta 19n/\Delta 19n}$ infected with Mm, but not in *dram1*$^{+/+}$ (Fig7 D). Next, we asked if the increased bacterial burden in Dram1-deficient larvae is dependent on Caspase 1 activity. Thus, we injected *caspase a* (a functional homologue of caspase 1) morpholino into the one cell stage of *dram1*$^{+/+}$ and *dram1*$^{\Delta 19/\Delta 19}$ embryos and infected with Mm at 1 dpf. In agreement with previous results (Fig 2), the infection burden of *dram1*$^{\Delta 19n/\Delta 19}$ embryos was higher that of *dram1*$^{+/+}$ (Fig7 E and F). Morpholino knockdown of *caspase a* knockdown in decreased infection burden in *dram1*$^{+/+}$ by 48% and in *dram1*$^{\Delta 19/\Delta 19}$ by 63%, bringing the infection burden of both groups to a similar low

level (Fig7 E and F). Collectively, these data suggest that mycobacterial infection in zebrafish embryos is promoted by pyroptosis of infected macrophages and that the lack of functional Dram1 results in macrophages being overgrown by the bacteria, thereby increasing pyroptotic cell death.

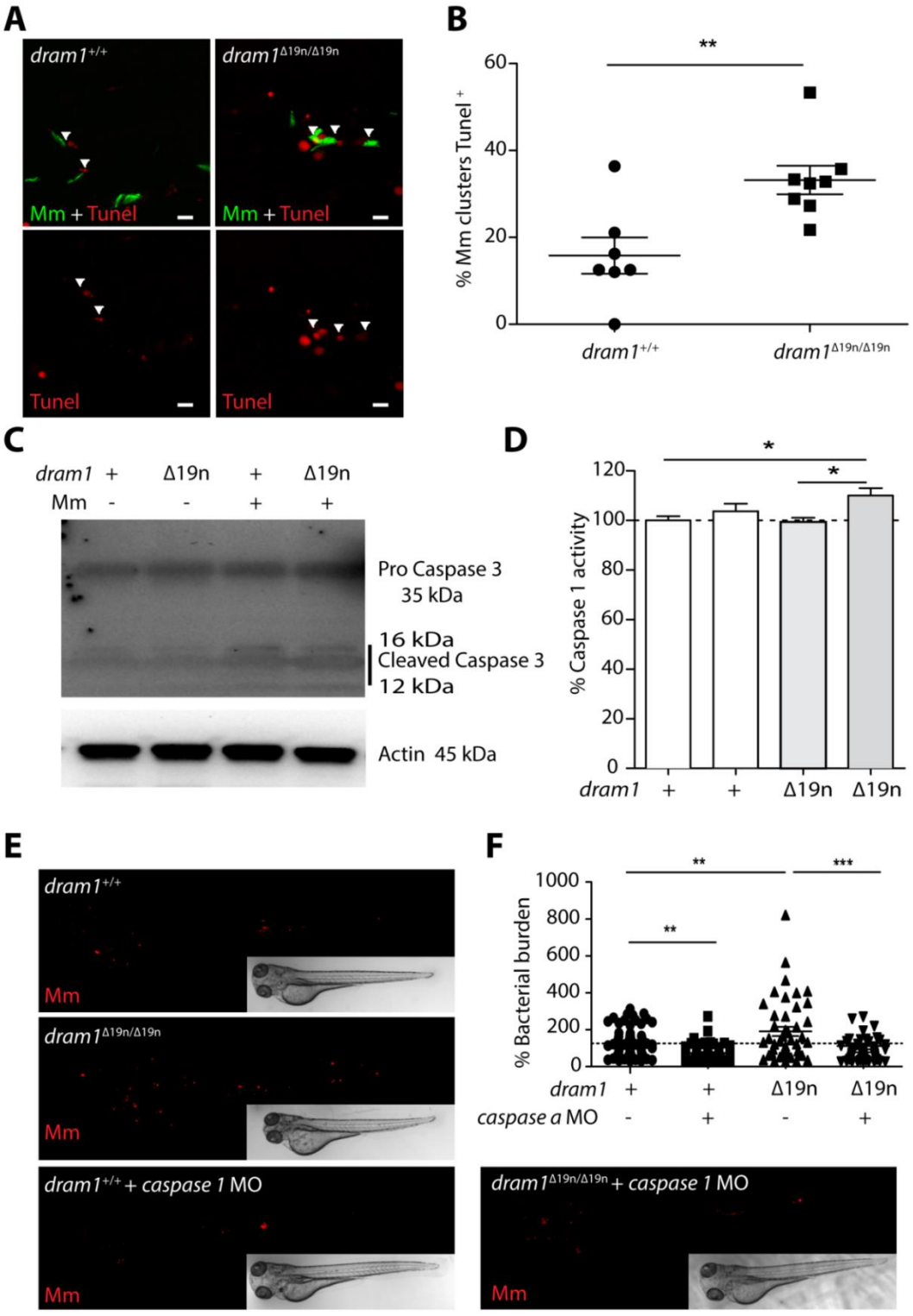

Figure 7: Dram1 deficiency results in increased Caspase 1-dependent programmed cell death

A. Representative confocal images of Tunel staining in *dram1*$^{\Delta 19n/\Delta 19n}$ and *dram1*$^{+/+}$ larvae at 2 dpi. The entire CHT region of 2 dpi fixed *dram1*$^{\Delta 19n/\Delta 19n}$ and *dram1*$^{+/+}$ larvae was imaged. The arrowheads indicate the cells positive for Tunel staining (Tunel^{+}). Scale bars, 10 µm.

B. Quantification of the percentage of Mm clusters Tunel^{+} in *dram1*$^{\Delta 19n/\Delta 19n}$ and *dram1*$^{+/+}$ larvae. Each dot represents the percentage of Mm clusters Tunel^{+} in the CHT region of an individual infected larva. ns, non-significant,*p<0.05,**p<0.01,***p<0.001.

C. Detection of pro-Caspase 3 and cleaved Caspase 3 protein in *dram1*$^{\Delta 19n/\Delta 19n}$ and *dram1*$^{+/+}$ embryos. Protein samples were extracted from 4 dpf infected and uninfected *dram1*$^{\Delta 19n/\Delta 19n}$ and *dram1*$^{+/+}$ larvae (>10 larvae/sample). The western blots were probed with antibodies against Caspase 3 and Actin as a loading control. The experiments were repeated two times.

D. Caspase 1 activity was assessed in *dram1*$^{\Delta 19n/\Delta 19n}$ and *dram1*$^{+/+}$/GFP-Lc3 embryos. Protein samples were obtained from 2 dpf infected and uninfected *dram1*$^{\Delta 19n/\Delta 19n}$ and *dram1*$^{+/+}$ embryos (>30 embryos/sample). The data is accumulated from two independent experiments. ns, non-significant,*p<0.05,**p<0.01,***p<0.001

E. Bacterial pixel counts were determined at 2 dpi following knockdown of *caspase a* in *dram1*$^{\Delta 19n/\Delta 19n}$ and *dram1*$^{+/+}$ embryos. The data is accumulated from two independent experiments. ns, non-significant,*p<0.05,**p<0.01,***p<0.001

F. Representative stereo images of infected *dram1*$^{\Delta 19n/\Delta 19n}$ and *dram1*$^{+/+}$ larvae at 2 dpi with and without *caspase a* MO injection**.**

Discussion

The lysosomal protein DRAM1 regulates autophagy and cell survival/death decisions under multiple stress conditions, including diseases like cancer and infection. Its mechanism of action remains largely unknown. In this study, we have demonstrated that mutation of *dram1* in zebrafish impairs resistance to mycobacterial infection. Importantly, we show that Dram1 deficiency reduces the acidification of Mm-containing vesicles, ultimately resulting in Caspase 1-dependent cell death of infected macrophages and increased extracellular growth of mycobacteria during early stages of the infection.

In this study we generated two independent *dram1* mutant lines using CRISPR/Cas9 technology to confirm and build upon results obtained with transient knockdown studies [7]. The combined use of knockdown (transient silencing) and knockout (stable loss of function) technologies is important, considering that targeting the same gene with these two approaches can result in

different phenotypes due to several reasons [61]. First, knockdown approaches can generate off-target effects and thereby induce phenotypes that are quite different from corresponding mutants. On the other hand, higher eukaryotic organisms can adapt to genetic variation (e.g. loss of function) by altering the activity of other genes, a mechanism which is called genetic compensation [62, 63]. This genetic compensation cannot be activated during transient knockdown of a gene and might therefore account for discrepancies between phenotypes resulting from knockout or knockdown approaches [62, 63]. Embryos and larvae homozygous for the two *dram1* CRISPR/Cas9 mutant alleles were viable and displayed no apparent phenotypes. Furthermore, we used the stable mutant lines to demonstrate that Dram1 deficiency does not affect development into adulthood or fertility. These observations are similar to *DRAM1* mutation in mouse models, which resulted in viable, fertile, and apparently normal individuals compared to their wild-type siblings (Mah thesis 2012) [86]. While DRAM1 deficiency was previously shown to affect the differentiation of neutrophils in acute promyelocytic leukaemia (APL) [48], the absence of functional Dram1 in zebrafish did not affect the total numbers of neutrophils or macrophages. In agreement with previous morpholino knockdown studies [7], both *dram1* mutant alleles showed increased susceptibility to mycobacterial infection in the zebrafish larval model of TB. The observation of a similar infection phenotype by two methods for disrupting *dram1* gene activity provides strong evidence that Dram1 is an important factor for host resistance against pathogenic mycobacteria. Furthermore, *dram1* mutants display decreased survival during *Salmonella* Typhimurium infection (Masud thesis) [87], indicating that Dram1 plays a role in immune defense against a broad range of intracellular bacterial pathogens.

The function of DRAM1 as a modulator of autophagy has been studied well *in vitro* [11]. We therefore tested whether zebrafish *dram1* mutants display defects in autophagic processes. Autophagy is a host response to diverse stress factors, including starvation. Wild type zebrafish larvae until 5 dpf can rely on their yolk proteins for nutrients [64], and we therefore assumed that their autophagic processes are not activated above a level normal for their developmental stage, unless autophagy is triggered by a stressor such as infection. In agreement, we did not detect any differences when comparing the basal levels of autophagy activity in uninfected *dram1* mutant larvae of 4 dpf to those of their wild type siblings. This finding is consistent with an *in*

vitro study of the function of mouse DRAM1 [65], which showed that basal autophagy was not altered in the absence of DRAM1 in primary mouse embryonic fibroblasts (MEFs). The five members of the DRAM family are conserved between human, mouse and zebrafish [7, 11, 66-68], and as also described in chapter 1 of this thesis. Therefore, it is conceivable that other DRAM family members can replace the loss of Dram1/DRAM1 under basal conditions, or that DRAM1 is only involved in autophagic processes in response to specific stress factors. Galavotti et al. (2013) found that autophagy induction in response to starvation or while blocking mTOR was not changed in the absence of DRAM1 [69]. However, the lack of DRAM1 affected the activation of autophagy in human cells (Hela and A549) following the induction of cellular stress by treatment with the mitochondria inhibitor 3-nitropropionic acid (3-NP) [49]. Besides infection, DNA-damage, and interference with impaired energy metabolism [7, 11, 13], it remains to be further investigated which stress factors can activate DRAM1/Dram1 *in vitro* and *in vivo*.

Treatment of *dram1* mutant larvae with BafA1, which blocks lysosomal degradation of autophagosomes, revealed an increase of GFP-Lc3 punctae and Lc3-II protein levels. This result is reminiscent of a previous study which showed that transient knockdown of human *DRAM1* significantly affected the clearance of autophagosomes in Hela cells [49]. The *dram1* mutants also accumulated higher Lc3-II protein levels than their wild type siblings under conditions of Mm infection. As in the case of BafA treatment, the accumulation of Lc3-II could indicate an increase in autophagosome production, or a defect in the degradation of autophagosomes. The latter possibility is supported by increased accumulation of ubiquitinated proteins in the *dram1* mutants. Collectively, we propose based on our data and the existing literature that the lysosomal protein Dram1/DRAM1 is important for maturation and degradation of autophagosomes. Furthermore, we believe that the induction of additional autophagosomes in response to BafA1 treatment or Mm infection – could function as a compensatory mechanism for the defect in degradation of cellular stress factors. Intriguingly, despite of the increased Lc3-II levels in infected *dram1* mutants, imaging in GFP-Lc3 transgenic fish revealed that mycobacteria are targeted by autophagic vesicles nearly 3-folds less frequently in *dram1* mutants than in wild type zebrafish larvae. This provides new evidence that Dram1 is required for autophagic defense against mycobacteria, as previously proposed based on morpholino

knockdown results [7]. How autophagic targeting of intracellular pathogens is orchestrated by DRAM1/Dram1 remains an important question for future research.

Previous studies have revealed that interaction occurs between autophagosomes and phagosomes [6, 70]. Specifically, defects in autophagy led to increased phagocytosis of Mtb in mouse macrophages [71]. Therefore, it was important to address the question whether altered autophagic targeting of Mm in zebrafish mutants was associated with different phagocytic ability of zebrafish macrophages. We found that, while Dram1 deficiency impaired autophagic defense against mycobacterial infection, it did not affect the capability of macrophages to phagocytose Mm. We did, however, find that Dram1 deficiency reduced autophagic targeting and acidification of Mm-containing vesicles, which ultimately resulted in the death of infected macrophages. These findings are in line with a recent study that revealed that DRAM1 directly mediates lysosomal membrane permeabilization (LMP) in HIV infected $CD4^+$ T cells [13]. Lysosome destabilisation triggered cell death and lowered viral replication [13]. While the mechanism of cell death could be similar in both situations, we detected higher mycobacterial burdens following death of the infected immune cells, as is to be expected from extracellularly growing Mm [23].

Apoptosis of infected cells is generally regarded as a host protective defence mechanism against mycobacterial infection, and virulent Mtb therefore actively inhibit apoptosis [33, 40, 72]. Apoptosis is a non-lytic form of cell death which prevents activation of an inflammatory response. Therefore, any intracellular mycobacteria will be encapsulated within the apoptotic envelope until the remains of the dying cell have been phagocytosed by recruited macrophages [40, 46, 73]. This is reasoned to be beneficial to the host by preventing uncontrolled extracellular growth of the bacteria. However, an *in vivo* study has demonstrated that apoptotic cell death can facilitate the expansion and dissemination of mycobacteria when macrophages phagocytosing the remains of the infected cell become infected themselves [23]. Nevertheless, only a small proportion of infected macrophages initiates apoptosis, as the majority of infected macrophages undergoes mycobacteria-induced lytic cell death [46]. In our study we observed that Caspase 3 was activated during mycobacterial infection, which is an indicator for apoptotic processes. DRAM1 was previously shown to mediate apoptosis by blocking the

degradation of the pro-apoptotic protein Bax [12]. While Dram1 deficiency leads to more cell death during Mm infection, we did not observe any changes in apoptosis activity on a whole embryo level, which led us to explore the role of Dram1 in other types of programmed cell death.

Strikingly, we found that Dram1 deficiency leads to more Caspase 1 activity and Caspase 1-dependent pyroptotic cell death. Pyroptosis is a lytic form of cell death which activates an inflammatory response [74]. Thus, the mechanisms, characteristics, and consequences of pyroptotic cell death are different from apoptosis [37, 75]. Previous studies revealed that pyroptosis can be induced by diverse pathogens and forms a critical mechanism to restrict microbial infection [75, 76]. In line with this, there is also evidence that mycobacteria inhibit pyroptosis of infected macrophages via diverse mechanisms [77]. However, recent studies found that lytic cell death (e.g. pyroptosis and necrosis) helps mycobacteria to evade host immunity and dissminate the infection [24, 46]. Indeed, in this present study we found that Caspase 1-dependent pyroptotic cell death promoted the expansion of bacteria. Moreover, genetic inhibition of Caspase 1 could rescue the exacerbated bacterial growth in *dram1* mutants. Taken together, the death of infected macrophages is intricately related to TB pathogenesis and can result either in increased dissemination or restriction of the infection. The sometimes contradicting evidence concerning the beneficial or detrimental effects of the different modes of cell death suggests that the context of cell death (e.g. location, timing during TB pathogenesis, and the immune status of the host) plays a crucial role in determining the outcome.

In conclusion, restriction of mycobacteria in infected macrophages during the early stages of infection requires functional Dram1. In this work, we have shown that Dram1 is involved in several processes important to defense against intracellular pathogens, potentially providing an intersection between modulation of autophagy, lysosomal function, and programmed cell death. Future studies are required to precisely elucidate the role of the lysosomal protein Dram1/DRAM1 in this network. Facing the complexity of the current TB situation, there is an urgent need to improve treatment strategies to control TB progression. Host-directed therapies (HDT) have emerged as a promising alternative to counter TB. HDTs can assist the host in

responding appropriately to Mtb infection, thereby promoting the effectiveness of drug treatments and reducing the time required for treatment [9]. Using an *in vivo* model for the early stages of TB disease we have demonstrated the importance of Dram1 for the elimination of intracellular mycobacteria and the cell fate of infected macrophages. This makes Dram1/DRAM1 – and its interaction partners that remain to be identified –promising targets for HDT development to improve the outcome of TB disease.

Materials and methods

Zebrafish culture and lines

Zebrafish lines in this study (TableS1) were maintained and used in compliance with local animal welfare regulations as overseen by the Leiden University (registration number: 10612). Embryos were kept in egg water, in a 28.5°C-30°C incubator, and treated with 0.02% Ethyl 3-aminobenzoate methanesulfonate (Tricaine, SIGMA-ALDRICH) in egg water for anesthesia before bacterial injections, imaging and fixation.

CRISPR/Cas9 mediated mutagenesis of zebrafish *dram1*

Single guide RNAs (sgRNAs) targeting the first coding exon of zebrafish *dram1* (ENSDARG00000045561) were designed using the chop-chop website [78]. To make sgRNAs, the template single strand DNA (ssDNA) (122 bases) was obtained by PCR complementation and amplification of full length ssDNA oligonucleotides. Oligonucleotides up to 81 nucleotides were purchased from Sigma-Aldrich using standard synthesis procedures (25 nmol concentration, purification with desalting method) (TableS2). The pairs of semi-complimentary oligos were annealed together by a short PCR program (50 µL reaction, 200uM dTNPs, 1 unit of Dream Taq polymerase (EP0703, ThermoFisher); PCR program: initial denaturation 95°C/3 minute (min), 5 amplification cycles 95°C/30 Second (s), 55°C/60 s, 72°C/30 s, final extension step 72°C/15 min) and subsequently the products were amplified using the primers in TableS2 with a standard PCR program (initial denaturation 95°C/3 min, 35 amplification cycles 95°C/30 s,55°C/60 s, 72°C/30 s, final extension step 72°C/15 min). The final PCR products were purified with Quick gel extraction

and PCR purification combo kit (00505495, ThermoFisher). The purified PCR products were confirmed by gel electrophoresis or Sanger sequencing (Base Clear, Netherlands). For *in vitro* transcription of sgRNAs, 0.2 µg template DNA was used to generate sgRNAs using the MEGA short script ®T7 kit (AM1354, ThermoFisher) and purified by RNeasy Mini Elute Clean up kit (74204, QIAGEN Benelux B.V., Venlo, Netherlands). The Cas9 mRNA was transcribed using mMACHINE® SP6 Transcription Kit (AM1340, ThermoFisher) from a Cas9 plasmid (39312, Addgene) (Hrucha et al 2013) and purified with RNeasy Mini Elute Clean up kit (74204,QIAGEN Benelux B.V., Venlo, Netherlands). A mixture of sgRNA and Cas9 mRNA was injected into one cell stage AB/TL embryos (sgRNA 150 pg/embryo and Cas9 mRNA 300 pg/embryo). The effect of CRISPR injection was confirmed by PCR and Sanger sequencing.

Genomic DNA isolation and genotyping

Genomic DNA was isolated from an individual embryo (2 dpf) or small pieces of the tail fin tissue of adults (>3 months) by fin clipping. Embryos or tissue samples were incubated in 200 µL 100% Methanol at -20°C overnight (O/N), then methanol was removed, and remaining methanol was evaporated at 70°C for 20 min. Next, samples were incubated in 25 µL of TE buffer containing 1.7 µg/µL proteinase K at 55°C for more than 5 h. Proteinase K was heat inactivated at 80°C for 30 min, after which samples were diluted with 100 µL of Milli-Q water. Genotyping was performed by PCR-amplification of the region of interest using the following primers: Forward: AGTGAACGTCCGTGTCTTTCTT, Reverse: ACATCTTGTCGATACAAAGCGA; followed by Sanger sequencing to identify mutations (Base Clear, Netherlands).

Western blot analysis

Embryos (4dpf/3dpi) were anaesthetised with Tricaine (Lot#MKBG4400V, SIGMA-ALDRICH) and homogenised with a Bullet-blender (Next-Advance) in RIPA buffer (#9806, Cell Signalling) containing a protein inhibitor cocktail (000000011836153001, cOmplete, Roche). The extracts were then spun down at 4°C for 10 min at 12000 rpm/min and the supernatants were frozen for storage at −80°C. Western blotting was performed using Mini-PROTEAN-TGX (456-9036, Bio-Rad) or 18% Tris-Hcl 18% polyacrylamide gels, and protein transfer to commercial PVDF membranes

(Trans-Blot Turbo-Transfer pack, 1704156, Bio-Rad). Membranes were blocked with 5% dry milk (ELK, Campina) in Tris buffered saline (TBS) solution with Tween 20 (TBST,1XTBS contains 0.1% Tween 20) buffer and incubated with primary and secondary antibodies. Digital images were acquired using Bio-Rad Universal Hood II imaging system (720BR/01565 UAS). Band intensities were quantified by densitometric analysis using Image Lab Software (Bio-Rad, USA) and values were normalised to actin as a loading control. Antibodies used were as follows: polyclonal rabbit anti DRAM1 (N-terminal) (ARP47432- P050, Aviva systems biology), polyclonal rabbit anti-Optineurin (C-terminal) (1:200, lot#100000; Cayman Chemical), polyclonal rabbit anti-p62 (C-terminal) (PM045, lot#019, MBL), polyclonal rabbit anti Lc3 (1:1000, NB100-2331, lot#AB-3, Novus Biologicals), monoclonal Caspase 3 antibody (1:1000, #9662, Lot#12, Cell Signaling), Anti mono-and polyubiquitinated conjugates mouse monoclonal antibody (1:200; BML-PW8810-0100, lot#01031445, Enzo life Sciences), Polyclonal actin antibody (1:1000, 4968S, lot#3, Cell Signaling), Anti-rabbit IgG, HRP-Linked Antibody (1:1000, 7074S, Lot#0026, Cell Signaling), Anti-mouse IgG, HRP-linked Antibody (1:3000, 7076S, Lot#029, Cell Signaling).

Infection conditions and bacterial burden quantification

Mycobacterium marinum strain M or *Mycobacterium marinum* strain 20 fluorescently labeled with Wasabi or mCherry, respectively [79, 80], were microinjected into the blood island of embryos at 28 hpf as previously described [81]. The injection dose was 200 CFU for all experiments, except for the phagocytosis assay (500 CFU). Embryos were manually dechorionated by tweezers and treated with tricaine to keep anesthesia before the injection. Infected embryos were imaged using a Leica MZ16FA stereo fluorescence microscope equipped with a DFC420C colour camera, and the bacterial pixels per infected fish data were obtained from the individual embryo stereo fluorescence images using previously described software [82].

Confocal laser scanning microscopy and image quantification

Fixed or live embryos were mounted with 1.5% low melting agarose (140727, SERVA) and imaged using a Leica TCS SPE confocal microscopy. For quantification of numbers of GFP-Lc3 positive vesicles, the fixed 4dpf larvae were imaged by confocal microscopy with a 63x water

immersion objective (NA 1.2) in the pre-defined tail fin region to detect the number of GFP-LC3-positive vesicles (Fig3 B and C). The numbers of GFP-Lc3 vesicles were measured by Fiji/ImageJ software (Fig3 B and C) [83]. For quantification of the autophagic response targeted to Mm clusters (Fig4 B and C), the fixed 2 dpi infected larvae were imaged by confocal microscopy with a 40X water immersion objective (NA 1.0) at over the whole caudal hematopoietic tissue (CHT) region. The percentage of Mm clusters that were positive for GFP-Lc3 per embryo was determined in this study. The same approach was used to quantify Mm acidification in the CHT region (Fig6 A and B). To investigate the intramacrophage or extracellular localization of bacteria, fixed 2 dpi larvae were again imaged over the CHT as described above, and first the number of Mm clusters was counted in this region and then the number of Mm clusters that were inside of macrophages were counted. To assay cell death, images from fixed 2 dpi larvae were acquired as above, and the number of Tunel staining^{+} cells in the CHT region was counted manually.

mRNA preparation and injection

dram1 or *dram1*$^{\Delta 19N}$ (negative control) RNA was isolated from wild type or *dram1*$^{\Delta 19n/\Delta 19n}$ embryos using QIAzol lysis reagent (79306, QIAGEN) and purified with the RNeasy MinElute Cleanup kit (74204, QIAGEN). cDNA synthesis was performed using the iScript cDNA synthesis kit (1708891, BIO-RAD). Full-length *dram1* cDNA and *dram1*$^{\Delta 19N}$ cDNA was obtained by PCR amplification using Phusion High-Fidelity DNA Polymerase (M0530S, New England Biolabs). The following primers were used: Forward: CTG CGG CGA GAT GTT TTG GTT; Reverse: CAA AAA CAG TGG GAC ATA CAG TGA A. *dram1* or *dram1*$^{\Delta 19N}$ PCR products were ligated into a ZERO BLUNT TOPO vector (450245, ThermoFisher) and the insert was confirmed by Sanger sequencing (Base Clear, Netherlands). *dram1* and *dram1*$^{\Delta 19N}$ mRNA was generated using the SP6 mMessage mMachine kit (AM1340, Thermo Fisher) and Poly(A) Tailing Kit (AM1350, ThermoFisher);purified using the RNeasy Min Elute Cleanup kit (74204, QIAGEN) and 50pg mRNA was microinjected into one cell stage embryos.

TUNEL assay

Cell death was examined by Terminal deoxynucleotidyl transferase dUTP nick end labelling

(TUNEL staining) with the In Situ Cell Death Detection Kit (000000011684795910, SIGMA-ALDRICH) in 2dpi fixed embryos. The assay was performed as follows: embryos were re-hydrated with 75% Methanol (MeOH)/5min, 50% MeOH/10 min, 25% MeOH/5 min, Wash 3× 5 min in PBS-TX. Then, embryos were permeabilized in 10 µg/mL Proteinase K for 40 min at 37 °C followed by a quick rinse in PBST. 50µl of reagents mixture was added per sample, incubated O/N at 37°C while protected from light. Samples were washed 3X with PBST for 15 min each time and stored in PBST. Samples were examined with confocal microscopy as described above.

LysoTracker staining and Myeloperoxidase (Mpx) activity assay

Infected embryos were immersed in egg water with 10 µM LysoTracker Red DND-99 (L7528, ThermoFisher) for 1h. Embryos were washed 3 times with egg water before imaging. Myeloperoxidase (Mpx) activity assay was performed with the Leukocyte detection Kit (390A, SIGMA-ALDRICH) for detection of neutrophils as previously described [82].

Drug treatment

Embryos were bath treated with Bafilomycin A1 (BafA1) (B1793-10UG, SIGMA-ALDRICH) diluted into egg water at the working concentration of 100 nM for 12h.

Caspase 1 activity assay

Caspase-1 activity was assayed with the fluorometric substrate Z-YVAD 7-Amido-4-trifluoromethylcoumarin (Z-YVAD-AFC, Caspase-1 Substrate IV, Colorimetric, sc-311283, Santa Cruz) as described previously [84] 20 embryos/group were lysed in hypotonic cell lysis buffer (25 mM 4-(2-hydroxyethyl) piperazine-1-ethanesulfonic acid, 5 mM ethylene glycol-bis (2-aminoethyl ether)-N,N,N',N'-tetraacetic acid, 5 mM dithiothreitol, 1:20 protease inhibitor cocktail (000000011836153001, cOmplete, Roche), pH 7.5) on ice for 10 min. For each reaction, 10 µg protein was incubated for 90 min at 28°C with 50 µM YVAD-AFC in 50 µl of reaction buffer (0.2% 3-[(3-cholamidopropyl) dimethylammonio]-1-propanesulfonate (CHAPS), 0.2 M 4-(2-hydroxyethyl) piperazine-1-ethanesulfonic acid, 20% sucrose, 29 mM dithiothreitol, pH 7.5). After the incubation, the fluorescence of the AFC released from the Z-YVAD-AFC substrate was

measured with a Microplate Readers (Tecan M1000) at an excitation wavelength of 400 and emission wavelength of 505 nm.

Morpholino Injection condition

caspase a morpholino (MO) in this study was previously used and validated [85] and purchased from Gene tools (Gene Tools, USA). MO oligonucleotide sequence: 5'GCCAT GTTTAGCTCAGGGCGCTGAC-3' [85]. MO was diluted in Milli-Q water with 0.05% phenol red and 1nL of 0.6 mM MO was microinjected into the yolk of one cell stage embryos as previously described.

Statistical analyses

Statistical analyses were performed using GraphPad Prism software (Version 5.01; GraphPad). All experimental data (mean ± SEM) was analyzed using unpaired, two-tailed t-tests for comparisons between two groups and one-way ANOVA with Tukey's multiple comparison methods as a posthoc test for comparisons between more than two groups. (ns, no significant difference; *$p < 0.05$; **$p < 0.01$; ***$p < 0.001$). For segregation from F1 or F3 heterozygous, data were analysed with a Chi-square test (ns, no significant difference).

Acknowledgements

We thank Daniel Klionsky for sharing of the GFP-Lc3 transgenic zebrafish line and George Lutfalla for the mpeg1-mCherryF line. We are grateful to all members of the fish facility team for zebrafish caretaking. We would like to thank Gerda Lamers and Joost Willemse for advice on confocal imaging and image analysis. R.Z. was supported by a grant from the China Scholarship Council (CSC). M.V. was funded by a European Marie Curie fellowship (H2020-MSCA-IF-2014-655424), V.T. was a Marie Curie fellow in the Initial Training Network FishForPharma (PITN-GA-2011-289209), and MvdV was supported by the Netherlands Technology Foundation TTW (project 13259).

References

1. Ahmad S, Mokaddas E. Recent advances in the diagnosis and treatment of multidrug-resistant tuberculosis. Respir Med 2009; 103:1777-90.

2. Gupta-Wright A, Tomlinson GS, Rangaka MX, Fletcher HA. World TB Day 2018: The Challenge of Drug Resistant Tuberculosis. F1000Res 2018; 7:217.

3. Yorimitsu T, Klionsky DJ. Autophagy: molecular machinery for self-eating. Cell Death Differ 2005; 12 Suppl 2:1542-52.

4. Watson RO, Manzanillo PS, Cox JS. Extracellular M. tuberculosis DNA targets bacteria for autophagy by activating the host DNA-sensing pathway. Cell 2012; 150:803-15.

5. Biswas D, Omar S Qureshi, Wing-Yiu Lee, Joanne E Croudace, Mura. M, Lammas DA. ATP-induced autophagy is associated with rapid killing of
intracellular mycobacteria within human monocytes/macrophages. BMC Immunology 2008; 9.

6. Gutierrez MG, Master SS, Singh SB, Taylor GA, Colombo MI, Deretic V. Autophagy is a defense mechanism inhibiting BCG and Mycobacterium tuberculosis survival in infected macrophages. Cell 2004; 119:753-66.

7. van der Vaart M, Korbee CJ, Lamers GE, Tengeler AC, Hosseini R, Haks MC, et al. The DNA damage-regulated autophagy modulator DRAM1 links mycobacterial recognition via TLR-MYD88 to autophagic defense [corrected]. Cell Host Microbe 2014; 15:753-67.

8. Kohler LJ, Roy CR. Autophagic targeting and avoidance in intracellular bacterial infections. Curr Opin Microbiol 2017; 35:36-41.

9. Wallis RS, Hafner R. Advancing host-directed therapy for tuberculosis. Nat Rev Immunol 2015; 15:255-63.

10. Kolloli A, Subbian S. Host-Directed Therapeutic Strategies for Tuberculosis. Front Med (Lausanne) 2017; 4:171.

11. Crighton D, Wilkinson S, O'Prey J, Syed N, Smith P, Harrison PR, et al. DRAM, a p53-induced modulator of autophagy, is critical for apoptosis. Cell 2006; 126:121-34.

12. Guan JJ, Zhang XD, Sun W, Qi L, Wu JC, Qin ZH. DRAM1 regulates apoptosis through increasing protein levels and lysosomal localization of BAX. Cell Death Dis 2015; 6:e1624.

13. Laforge M, Limou S, Harper F, Casartelli N, Rodrigues V, Silvestre R, et al. DRAM triggers

lysosomal membrane permeabilization and cell death in CD4(+) T cells infected with HIV. PLoS Pathog 2013; 9:e1003328.

14. Lee J, Repasy T, Papavinasasundaram K, Sassetti C, Kornfeld H. Mycobacterium tuberculosis induces an atypical cell death mode to escape from infected macrophages. PLoS One 2011; 6:e18367.

15. McClean CM, Tobin DM. Macrophage form, function, and phenotype in mycobacterial infection: lessons from tuberculosis and other diseases. Pathog Dis 2016; 74.

16. Sundaramurthy V, Korf H, Singla A, Scherr N, Nguyen L, Ferrari G, et al. Survival of Mycobacterium tuberculosis and Mycobacterium bovis BCG in lysosomes in vivo. Microbes Infect 2017; 19:515-26.

17. Romagnoli A, Etna MP, Giacomini E, Pardini M, Remoli ME, Corazzari M, et al. ESX-1 dependent impairment of autophagic flux by Mycobacterium tuberculosis in human dendritic cells. Autophagy 2012; 8:1357-70.

18. Deretic V, Levine B. Autophagy, immunity, and microbial adaptations. Cell Host Microbe 2009; 5:527-49.

19. Levine B. Eating oneself and uninvited guests: autophagy-related pathways in cellular defense. Cell 2005; 120:159-62.

20. Franco LH, Nair VR, Scharn CR, Xavier RJ, Torrealba JR, Shiloh MU, et al. The Ubiquitin Ligase Smurf1 Functions in Selective Autophagy of Mycobacterium tuberculosis and Anti-tuberculous Host Defense. Cell Host Microbe 2017; 21:59-72.

21. Manzanillo PS, Ayres JS, Watson RO, Collins AC, Souza G, Rae CS, et al. The ubiquitin ligase parkin mediates resistance to intracellular pathogens. Nature 2013; 501:512-6.

22. Ponpuak M, Davis AS, Roberts EA, Delgado MA, Dinkins C, Zhao Z, et al. Delivery of cytosolic components by autophagic adaptor protein p62 endows autophagosomes with unique antimicrobial properties. Immunity 2010; 32:329-41.

23. Davis JM, Ramakrishnan L. The role of the granuloma in expansion and dissemination of early tuberculous infection. Cell 2009; 136:37-49.

24. Mahamed D, Boulle M, Ganga Y, Mc Arthur C, Skroch S, Oom L, et al. Intracellular growth of Mycobacterium tuberculosis after macrophage cell death leads to serial killing of host cells.

Elife 2017; 6.

25. Cambier CJ, O'Leary SM, O'Sullivan MP, Keane J, Ramakrishnan L. Phenolic Glycolipid Facilitates Mycobacterial Escape from Microbicidal Tissue-Resident Macrophages. Immunity 2017; 47:552-65 e4.

26. Berg RD, Levitte S, O'Sullivan MP, O'Leary SM, Cambier CJ, Cameron J, et al. Lysosomal Disorders Drive Susceptibility to Tuberculosis by Compromising Macrophage Migration. Cell 2016; 165:139-52.

27. Cambier CJ, Falkow S, Ramakrishnan L. Host evasion and exploitation schemes of Mycobacterium tuberculosis. Cell 2014; 159:1497-509.

28. Sandor M, Weinstock JV, Wynn TA. Granulomas in schistosome and mycobacterial infections: a model of local immune responses. TRENDS in Immunology 2003; 24.

29. Flynn JL, Chan J, Lin PL. Macrophages and control of granulomatous inflammation in tuberculosis. Mucosal Immunol 2011; 4:271-8.

30. Ehlers S, Schaible UE. The granuloma in tuberculosis: dynamics of a host-pathogen collusion. Front Immunol 2012; 3:411.

31. Silva Miranda M, Breiman A, Allain S, Deknuydt F, Altare F. The tuberculous granuloma: an unsuccessful host defence mechanism providing a safety shelter for the bacteria? Clin Dev Immunol 2012; 2012:139127.

32. Ndlovu H, Marakalala MJ. Granulomas and Inflammation: Host-Directed Therapies for Tuberculosis. Front Immunol 2016; 7:434.

33. Ramakrishnan L. Revisiting the role of the granuloma in tuberculosis. Nat Rev Immunol 2012; 12:352-66.

34. Cronan MR, Beerman RW, Rosenberg AF, Saelens JW, Johnson MG, Oehlers SH, et al. Macrophage Epithelial Reprogramming Underlies Mycobacterial Granuloma Formation and Promotes Infection. Immunity 2016; 45:861-76.

35. Srinivasan L, Ahlbrand S, Briken V. Interaction of Mycobacterium tuberculosis with host cell death pathways. Cold Spring Harb Perspect Med 2014; 4.

36. Elmore S. Apoptosis: A Review of Programmed Cell Death. Toxicol Pathol 2007; 35:495–516.

37. Fink SL, Cookson BT. Apoptosis, pyroptosis, and necrosis: mechanistic description of dead and dying eukaryotic cells. Infect Immun 2005; 73:1907-16.

38. Galluzzi L, Vitale I, Aaronson SA, Abrams JM, Adam D, Agostinis P, et al. Molecular mechanisms of cell death: recommendations of the Nomenclature Committee on Cell Death 2018. Cell Death Differ 2018; 25:486-541.

39. Mauro Oddo TR, Antoine Attinger, Talitha Bakker, H. Robson MacDonald and Pascal R. A. Meylan. Fas Ligand-Induced Apoptosis of Infected Human Macrophages Reduces the Viability of Intracellular Mycobacterium tuberculosis. J Immunol 1998; 160:5448-54.

40. Behar SM, Martin CJ, Booty MG, Nishimura T, Zhao X, Gan HX, et al. Apoptosis is an innate defense function of macrophages against Mycobacterium tuberculosis. Mucosal Immunol 2011; 4:279-87.

41. Aguilo N, Marinova D, Martin C, Pardo J. ESX-1-induced apoptosis during mycobacterial infection: to be or not to be, that is the question. Front Cell Infect Microbiol 2013; 3:88.

42. Roca FJ, Ramakrishnan L. TNF dually mediates resistance and susceptibility to mycobacteria via mitochondrial reactive oxygen species. Cell 2013; 153:521-34.

43. Stutz MD, Ojaimi S, Allison C, Preston S, Arandjelovic P, Hildebrand JM, et al. Necroptotic signaling is primed in Mycobacterium tuberculosis-infected macrophages, but its pathophysiological consequence in disease is restricted. Cell Death Differ 2017.

44. Lamkanfi M, Dixit VM. Manipulation of host cell death pathways during microbial infections. Cell Host Microbe 2010; 8:44-54.

45. Amaral EP, Ribeiro SC, Lanes VR, Almeida FM, de Andrade MR, Bomfim CC, et al. Pulmonary infection with hypervirulent Mycobacteria reveals a crucial role for the P2X7 receptor in aggressive forms of tuberculosis. PLoS Pathog 2014; 10:e1004188.

46. Stutz MD, Clark MP, Doerflinger M, Pellegrini M. Mycobacterium tuberculosis: Rewiring host cell signaling to promote infection. J Leukoc Biol 2018; 103:259-68.

47. He C, Clinton R. Bartholomew, Weibin Zhou, Klionsky aDJ. Assaying autophagic activity in transgenic GFP-Lc3 and GFPGabarap
zebrafish embryos. Autophagy 2009; 5:520-6.

48. Humbert M, Mueller C, Fey MF, Tschan MP. Inhibition of damage-regulated autophagy

modulator-1 (DRAM-1) impairs neutrophil differentiation of NB4 APL cells. Leuk Res 2012; 36:1552-6.

49. Zhang XD, Qi L, Wu JC, Qin ZH. DRAM1 regulates autophagy flux through lysosomes. PLoS One 2013; 8:e63245.

50. Barth S, Glick D, Macleod KF. Autophagy: assays and artifacts. J Pathol 2010; 221:117-24.

51. Klionsky DJ, Hagai Abeliovich, Patrizia Agostinis, Devendra K. Agrawal, Aliev G. Guidelines for the use and interpretation of assays for monitoring
autophagy in higher eukaryotes. Autophagy 2008; 4:151-75.

52. Mauvezin C, Neufeld TP. Bafilomycin A1 disrupts autophagic flux by inhibiting both V-ATPase-dependent acidification and Ca-P60A/SERCA-dependent autophagosome-lysosome fusion. Autophagy 2015; 11:1437-8.

53. Ying H, Turturro S, Nguyen T, Shen X, Zelkha R, Johnson EC, et al. Induction of autophagy in rats upon overexpression of wild-type and mutant optineurin gene. BMC Cell Biol 2015; 16:14.

54. Myeku N, Figueiredo-Pereira ME. Dynamics of the degradation of ubiquitinated proteins by proteasomes and autophagy: association with sequestosome 1/p62. J Biol Chem 2011; 286:22426-40.

55. Bjorkoy G, Lamark T, Brech A, Outzen H, Perander M, Overvatn A, et al. p62/SQSTM1 forms protein aggregates degraded by autophagy and has a protective effect on huntingtin-induced cell death. J Cell Biol 2005; 171:603-14.

56. Klionsky DJ, Abdelmohsen K, Abe A, Abedin MJ, Abeliovich H, Acevedo Arozena A, et al. Guidelines for the use and interpretation of assays for monitoring autophagy (3rd edition). Autophagy 2016; 12:1-222.

57. Bernut A, Herrmann JL, Kissa K, Dubremetz JF, Gaillard JL, Lutfalla G, et al. Mycobacterium abscessus cording prevents phagocytosis and promotes abscess formation. Proc Natl Acad Sci U S A 2014; 111:E943-52.

58. Miao EA, Rajan JV, Aderem A. Caspase-1-induced pyroptotic cell death. Immunol Rev 2011; 243:206-14.

59. Kyrylkova K, Kyryachenko S, Leid M, Kioussi C. Detection of apoptosis by TUNEL assay. Methods Mol Biol 2012; 887:41-7.

60. Porter AG, Janicke RU. Emerging roles of caspase-3 in apoptosis. Cell Death and Differentiation 1999; 6.

61. Stainier DYR, Raz E, Lawson ND, Ekker SC, Burdine RD, Eisen JS, et al. Guidelines for morpholino use in zebrafish. PLoS Genet 2017; 13:e1007000.

62. El-Brolosy MA, Stainier DYR. Genetic compensation: A phenomenon in search of mechanisms. PLoS Genet 2017; 13:e1006780.

63. Rossi A, Kontarakis Z, Gerri C, Nolte H, Holper S, Kruger M, et al. Genetic compensation induced by deleterious mutations but not gene knockdowns. Nature 2015; 524:230-3.

64. Quinlivan VH, Farber SA. Lipid Uptake, Metabolism, and Transport in the Larval Zebrafish. Front Endocrinol (Lausanne) 2017; 8:319.

65. Nagata M, Arakawa S, Yamaguchi H, Torii S, Endo H, Tsujioka M, et al. Dram1 regulates DNA damage-induced alternative autophagy. Cell Stress 2018; 2:55-65.

66. Mrschtik M, Ryan KM. Lysosomal proteins in cell death and autophagy. FEBS J 2015; 282:1858-70.

67. Chung J, Nakatsu F, Baskin JM, De Camilli P. Plasticity of PI4KIIIalpha interactions at the plasma membrane. EMBO Rep 2015; 16:312-20.

68. Park SM, Kim K, Lee EJ, Kim BK, Lee TJ, Seo T, et al. Reduced expression of DRAM2/TMEM77 in tumor cells interferes with cell death. Biochem Biophys Res Commun 2009; 390:1340-4.

69. Galavotti S, Bartesaghi S, Faccenda D, Shaked-Rabi M, Sanzone S, McEvoy A, et al. The autophagy-associated factors DRAM1 and p62 regulate cell migration and invasion in glioblastoma stem cells. Oncogene 2013; 32:699-712.

70. Deretic V, Levine B. Autophagy balances inflammation in innate immunity. Autophagy 2018:1-9.

71. Bonilla DL, Bhattacharya A, Sha Y, Xu Y, Xiang Q, Kan A, et al. Autophagy regulates phagocytosis by modulating the expression of scavenger receptors. Immunity 2013; 39:537-47.

72. Gan H, Lee J, Ren F, Chen M, Kornfeld H, Remold HG. Mycobacterium tuberculosis blocks crosslinking of annexin-1 and apoptotic envelope formation on infected macrophages to maintain virulence. Nat Immunol 2008; 9:1189-97.

73. Martin CJ, Booty MG, Rosebrock TR, Nunes-Alves C, Desjardins DM, Keren I, et al. Efferocytosis is an innate antibacterial mechanism. Cell Host Microbe 2012; 12:289-300.

74. Wallach D, Kang TB, Dillon CP, Green DR. Programmed necrosis in inflammation: Toward identification of the effector molecules. Science 2016; 352:aaf2154.

75. Bergsbaken T, Fink SL, Cookson BT. Pyroptosis: host cell death and inflammation. Nat Rev Microbiol 2009; 7:99-109.

76. Cookson B, Brennan M. Pro-inflammatory programmed cell death. TRENDS in Microbiology 2001; 9:113-4.

77. Danelishvili L, Everman JL, McNamara MJ, Bermudez LE. Inhibition of the Plasma-Membrane-Associated Serine Protease Cathepsin G by Mycobacterium tuberculosis Rv3364c Suppresses Caspase-1 and Pyroptosis in Macrophages. Front Microbiol 2011; 2:281.

78. Labun K, Montague TG, Gagnon JA, Thyme SB, Valen E. CHOPCHOP v2: a web tool for the next generation of CRISPR genome engineering. Nucleic Acids Res 2016; 44:W272-6.

79. van der Sar AM, Abdallah AM, Sparrius M, Reinders E, Vandenbroucke-Grauls CM, Bitter W. Mycobacterium marinum strains can be divided into two distinct types based on genetic diversity and virulence. Infect Immun 2004; 72:6306-12.

80. Takaki K, Davis JM, Winglee K, Ramakrishnan L. Evaluation of the pathogenesis and treatment of Mycobacterium marinum infection in zebrafish. Nat Protoc 2013; 8:1114-24.

81. Benard EL, van der Sar AM, Ellett F, Lieschke GJ, Spaink HP, Meijer AH. Infection of zebrafish embryos with intracellular bacterial pathogens. J Vis Exp 2012.

82. Cui C, Benard EL, Kanwal Z, Stockhammer OW, van der Vaart M, Zakrzewska A, et al. Infectious disease modeling and innate immune function in zebrafish embryos. Methods Cell Biol 2011; 105:273-308.

83. Schindelin J, Arganda-Carreras I, Frise E, Kaynig V, Longair M, Pietzsch T, et al. Fiji: an open-source platform for biological-image analysis. Nat Methods 2012; 9:676-82.

84. Tyrkalska SD, Candel S, Angosto D, Gomez-Abellan V, Martin-Sanchez F, Garcia-Moreno D, et al. Neutrophils mediate Salmonella Typhimurium clearance through the GBP4 inflammasome-dependent production of prostaglandins. Nat Commun 2016; 7:12077.

85. Masumoto J, Zhou W, Chen FF, Su F, Kuwada JY, Hidaka E, et al. Caspy, a zebrafish

caspase, activated by ASC oligomerization is required for pharyngeal arch development. J Biol Chem 2003; 278:4268-76.

86. Mah LY. *Characterisation of DRAM-1 in vitro and in vivo*. University of Glasgow, 2012:263.

87. Samrah M. Autophagy and Lc3-associated phagocytosis in host defense against *Salmonella.* Leiden University, 2017:233.

Supplementary data

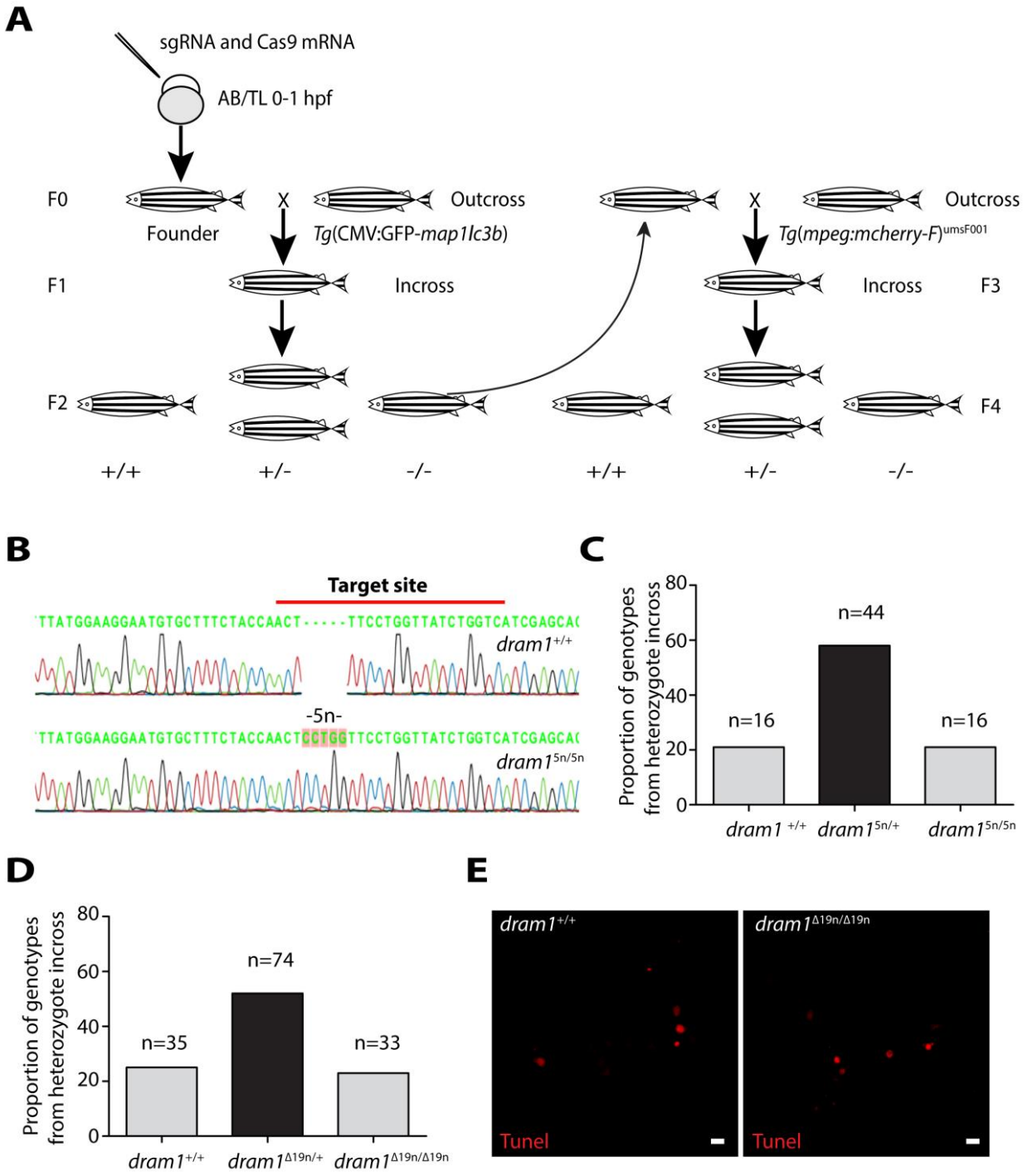

Supplementary figure 1: Dram1 deficiency does not result in apparent defects in development or survival

A. Schematic diagram showing the workflow used for the generation of *dram1* mutant lines. Target-specific sgRNA and Cas9 mRNA were co-injected into one cell stage embryos (AB/TL, wild type line). Founders were outcrossed to

Tg(*CMV:EGFP-map1lc3b*) or wild type fish to obtain F1. After 3-4 months, the F1 was incrossed to obtain homozygous mutant and wild type F2 siblings. *dram1*$^{\Delta 19n/\Delta 19n}$ were outcrossed with the macrophage marker *Tg*(*mpeg1:mCherry-F*)^{umsF001} and after 3-4 months subsequently incrossed to obtain *dram1*$^{+/+}$, *dram1*$^{\Delta 19/+}$, and *dram1*$^{\Delta 19n/\Delta 19n}$ carrying *Tg*(*mpeg1:mCherry-F*)^{umsF001}.

B. Sanger sequencing of *dram1*$^{+/+}$ and *dram1*$^{5n/5n}$ from F2 fish. The red line indicates the CRISPR/Cas9 target site. The genomic DNA was isolated from fin tissue of adults (>3 months old). The *dram1*$^{5n/5n}$ sequence revealed insertion of 5 nucleotides within the target site.

C. Segregation from *dram1*$^{5N/+}$ F1 heterozygous incross. Genotypes of adult fish (>3 months old) combined from at least three independent breedings were confirmed by PCR and Sanger sequencing. Data were analyzed by Chi square test. ns, non-significant,*p<0.05,**p<0.01,***p<0.001

D. Segregation from *dram1*$^{\Delta 19n+}$*/mpeg1:mCherry-F* F1 heterozygous incross. Genotypes of adult fish (>3 months old) combined from at least three independent breedings were confirmed by PCR and sequencing. Data were analyzed by Chi square test. ns, non-significant,*p<0.05,**p<0.01,***p<0.001

E. Representative confocal micrographs tail region of Tunel staining performed on *dram1*$^{\Delta 19n/\Delta 19n}$ and *dram1*$^{+/+}$ larvae at 3dpf. Scale bar, 10 μm.

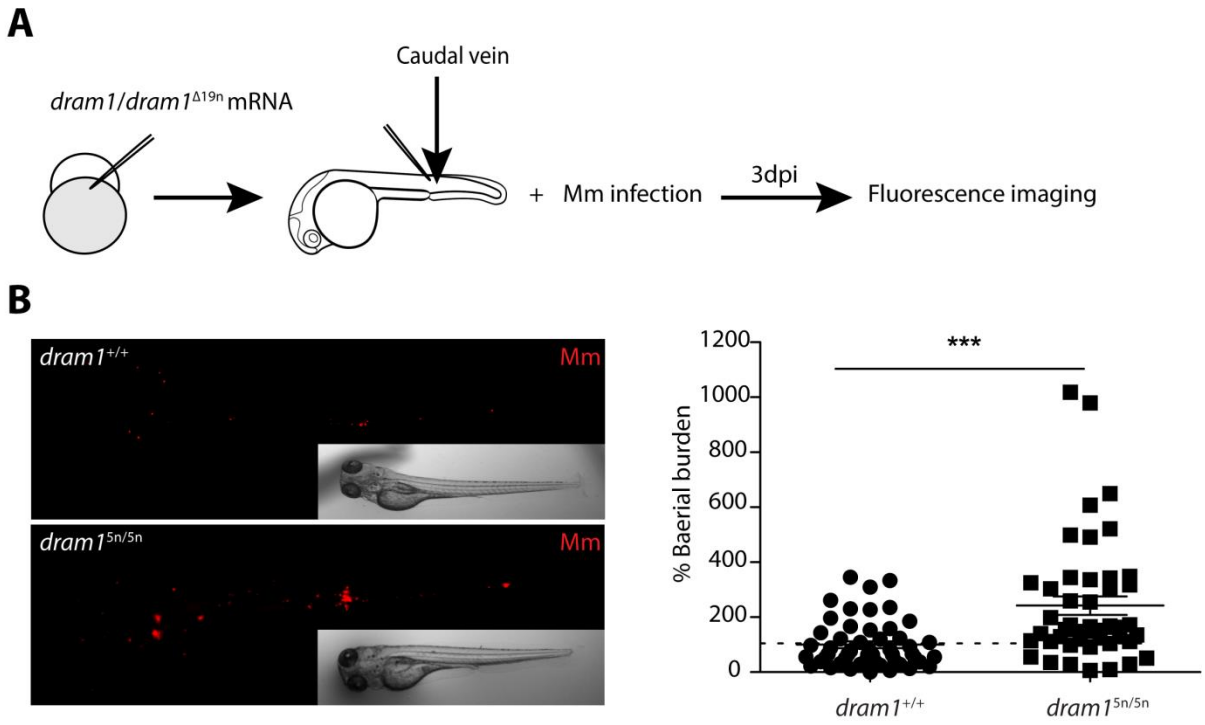

Supplementary figure 2: Dram1 is required for the host to restrict Mm infection

A. Workflow representing the experimental design for Mm infection experiments. Bacterial pixel counts were examined at 3 dpi.

B. Representative stereo images of infected *dram1*$^{+/+}$ and *dram1*$^{5n/5n}$ larvae at 3 dpi**.**

C. Bacterial burdens were determined at 3 dpi. The data is accumulated from two independent experiments. Each dot represents an individual larva. ns, non-significant, *p<0.05, **p<0.01, ***p<0.001

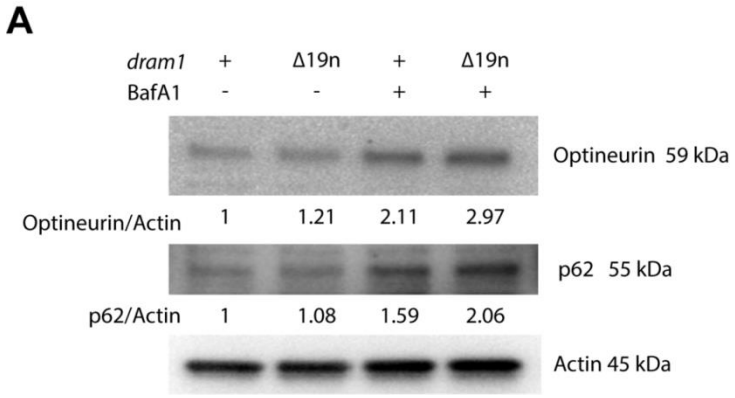

Supplementary figure 3: Increased accumulation of p62 and Optineurin suggests that autophagic flux is decreased without Dram1

A. p62 and Optineurin protein levels were detected in *dram1*$^{\Delta 19n/\Delta 19n}$ and *dram1*$^{+/+}$ larvae in absence or presence of BafA1. Protein samples were extracted from 4dpf *dram1*$^{\Delta 19n/\Delta 19n}$ and *dram1*$^{+/+}$ larvae (>10 larvae/sample). The blots were probed with antibodies against p62, Optineurin, and Actin as a loading control. p62/Actin and Optineurin/Actin. The ratios are indicated below the blot.

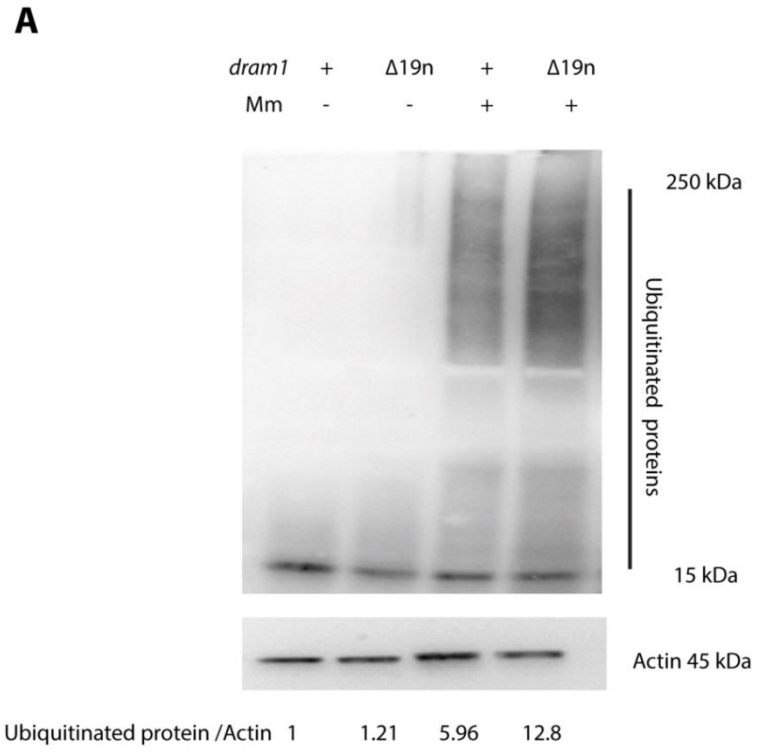

Supplementary figure 4: Accumulation of ubiquitinated proteins in *dram1*$^{+/+}$ and *dram1*$^{\Delta 19n/\Delta 19n}$ during Mm infection

A. Detection of ubiquitination in infected and uninfected larvae. Protein samples were extracted from 4dpf/3dpi *dram1*$^{\Delta 19n/\Delta 19n}$ and *dram1*$^{+/+}$ larvae (>10 larvae/sample). The blots were probed with antibodies against poly and mono ubiquitin; Actin was used as a loading control. Ubiquitinated protein/Actin ratios are indicated below the blot.

Supplementary table1: The zebrafish lines used in this study

Name	Description	Reference
AB/TL	Wild type strain	7
Tg(*CMV:EGFP-map1lc3b*)	GFP reporter transgenic zebrafish for Lc3	47
Tg(*mpeg1:mCherryF*)^{umsF001}	Macrophage marker with membrane-localizing *mCherry-F*	57
dram1$^{+/+}$/GFP-Lc3	Siblings of *dram1* carrying a transgenic GFP-Lc3 reporter	In this study
dram1$^{\Delta 19n/\Delta 19n}$/GFP-Lc3	*dram1* mutant line (Δ19n indel) carrying a transgenic GFP-Lc3 reporter	In this study
dram1$^{5n/5n}$/GFP-Lc3	*dram1* mutant line (5n indel) carrying a transgenic GFP-Lc3 reporter	In this study
dram1$^{+/+}$*/mpeg1:mCherry-F*	Siblings of *dram1*$^{\Delta 19n/\Delta 19n}$ carrying a transgenic *mpeg1:mCherry-F* reporter	In this study
dram1$^{\Delta 19n/\Delta 19n}$*/mpeg1:mCherry-F*	Siblings of *dram1*$^{+/+}$ carrying a transgenic *mpeg1:mCherry-F* reporter	In this study

Supplementary table2: Primers for complementation and amplification of sgRNA

Name	Forward (5'-3')	Reverse (5'-3')
dram1 sgRNA template	GCG**TAATACGACTCACTATAG**GACCAGATAA CCAGGAAAGTTGGTTTTAGAGCTAGAAATAG CAAGTTAAAATAAGGCTAGTC	GATCCGCACCGACTCGGTGCCACTTTTTCAA GTTGATAACGGACTAGCCTTATTTTAACTTG CTATTTCTAGCTCTAAAAC
sg RNA amplify	GCGTAATACGACTCACTATAG	GATCCGCACCGACTCGGT

T7 promoter: **TAATACGACTCACTATAG**

The underlined sequence indicates the target sites for gRNAs designed to mutate *dram1*